1   Reduction in sunlit Earth reflected radiance 317 to 780 nm during the eclipse of 21 August 2017

2   Jay Herman[1], Guoyong Wen[2], Alexander Marshak[3], Karin Blank[3], Liang Huang[4], Alexander Cede[5], Nader

3   Abuhassan[1], Matthew Kowalewski[6]

4   Abstract

5   Ten wavelength channels of calibrated radiance image data from the sunlit Earth are obtained

6   every 65 minutes during Northern Hemisphere summer from the DSCOVR/EPIC instrument located near

7   the Earth-Sun Lagrange-1 point (L_1), 1.5 million km from the Earth. The L_1 location permitted seven

8   observations of the Moon's shadow on the Earth for about 3 hours during the 21 August 2017 eclipse.

9   Two of the observations were timed to coincide with totality over Casper, Wyoming and Columbia,

10   Missouri. Since, the solar irradiances within 5 channels (λ_i = 388, 443, 551, 680, and 780 nm) are not

11   strongly absorbed in the atmosphere, they can be used for characterizing eclipse reduction in reflected

12   radiances for the sunlit face of the Earth containing the eclipse shadow. Five channels (λ_i= 317.5, 325,

13   340, 688, and 764 nm) that are partially absorbed in the atmosphere give consistent reductions

14   compared to the non-absorbed channels. This indicates that cloud reflectivities dominate the 317.5 to

15   780 nm radiances reflected back to space from the sunlit Earth's disk with a strong contribution from

16   Rayleigh scattering for the shorter wavelengths. A reduction of 10 % in the spectrally integrated

17   radiance (387 to 781 nm) reflected from the sunlit Earth towards L_1 was obtained for two sets of

18   observations on 21 August 2017, while the shadow was in the vicinity of Casper, Wyoming (42.8666° N,

19   106.3131° W, centered on 17:44:50 UTC) and Columbia, Missouri (38.9517° N, 92.3341° W, centered on

20   18:14:50 UTC). In contrast, when non-eclipse days (20 Aug. and 23 Aug.) are compared for each

21   wavelength channel, the change in reflected light is much smaller (less than 1 % for 443 nm compared to

22   9 % (Casper) and 8 % (Columbia) during the eclipse). Also measured was the ratio $R_{EN}(\lambda_i)$ of reflected

23   radiance on adjacent non-eclipse days divided by radiances centered in the eclipse totality region with

24   the same geometry for all 10 wavelength channels. The measured $R_{EN}(443\ nm)$ was smaller for Columbia

25   (169) than for Casper (935), because Columbia had more cloud cover than Casper. $R_{EN}(\lambda_i)$ forms a useful

26   test of 3-D radiative transfer models for an eclipse in the presence of optically thin clouds. Specific

27   values measured at Casper with thin clouds are $R_{EN}(340\ nm)$ = 475, $R_{EN}(388\ nm)$ = 3500, $R_{EN}(443\ nm)$ =

28   935, $R_{EN}(551\ nm)$ = 5455, $R_{EN}(680\ nm)$ = 220, and $R_{EN}(780\ nm)$ = 395. Some of the variability is caused by

29   changing cloud amounts within the moving region of totality during the 2.7 minutes needed to measure

30   each wavelength channel.

31   Keywords: Atmospheric Processes, Eclipse, DSCOVR/EPIC, Reflected Energy

32   **Correspondence email: jay.r.herman@nasa.gov**

33   **[1]University of Maryland Baltimore County JCET**

34   **[2]Morgan State University, Baltimore Maryland**

35   **[3]NASA Goddard Space Flight Center, Greenbelt, Maryland**

36   **[4]Science Systems and Applications, Lanham, Maryland**

37   **[5]Goddard Earth Sciences Technology & Research (GESTAR) Columbia, Columbia, MD 21046, USA**

38   **[6]SciGlob Instruments and Services, Elkridge, Maryland USA**

1.0 Introduction

Measured radiances of the entire sunlit Earth were obtained during the 21 August 2017 eclipse from EPIC (Earth Polychromatic Imaging Camera) on the DSCOVR (Deep Space Climate Observatory) satellite. DSCOVR obtains synoptic observations of the Earth from an orbit around the L_1 point (Lagrange 1) 1.5 million km from Earth (Herman et al., 2018). This study focuses on data from two selected locations during the 21 August 2017 eclipse that crossed the United States from west to east. The locations selected were Casper, Wyoming and Columbia, Missouri, both near the center of the path of totality and both with a nearly overhead total solar eclipse (local time 11:45 in Casper, Wyoming and 13:12 in Columbia, Missouri). The sites were selected in advance to have a high probability of almost cloud-free skies, and so that totality would occur about 30 minutes apart in UTC (Coordinated Universal Time) to accommodate the satellite's ability to acquire data. On the day of the eclipse, Casper, Wyoming had almost clear skies (Fig. 1), with some high thin clouds visible, while Columbia, Missouri had thin low altitude cloud cover (Fig. 2).

Observations of total solar eclipses have been made with varying degrees of sophistication for thousands of years as reviewed by Littman et al. (2008). At a given location, observations of reduced irradiance reaching the Earth's surface are limited to just a few minutes of totality and about two hours of partial obscuration (Meeus, 2003). The totality region (umbra) is an oval of about 110 -120 km in size near local noon at Casper, Wyoming and Columbia, Missouri, but will change size and shape as a function of local solar zenith angle (https://eclipse2017.nasa.gov/eclipse-maps). Some of the complicating factors concerning quantitative eclipse observations include the effects of the solar corona and light scattered in the atmosphere (Liendo, and Chacin, 2004; Emde and Mayer, 2007).

A detailed analysis of an eclipse that occurred in 2006 over southern Europe includes both ground-based and space-based polar orbiting MODIS (Moderate Resolution Imaging Spectroradiometer) observations of cloud cover before totality (Gerasopoulos et al., 2008) as well as theoretical modelling of the eclipse, but unlike the present study, it was largely limited to local effects near the region of totality. A comparison from a meteorological radiation model and measurements of total solar irradiance were made near Athens Greece (84 % of a total eclipse) that showed good agreement in the presence of light clouds (Psiloglou and Kambezidis, 2007). A 3D Monte Carlo radiative transfer study (Emde and Mayer, 2007) was applied to the geometry for the nearly overhead total eclipse of 29 March 2006 (13:20 local time in Turkey) to estimate the downward global radiation at the surface, but without the effect of clouds included in the calculation. An application of the 3D model to the 2006 eclipse over Kastelorizo, Greece with fairly cloud-free measurements (few cumulus, 1-2 octas, and scattered cirrus, 3-4 octas) at 380 nm showed good agreement for the ratio (ratio = 217) of global surface irradiance starting 5 minutes before totality to that during totality (Kazantzidis et al., 2007). Successful modelling of the light levels during an eclipse under realistic conditions is the first step to improved modelling of high cloud reflection and shadowing of solar radiation on the Earth's energy balance.

The observations from the DSCOVR satellite are part of a larger project that combines simultaneously obtained satellite and ground-based measurements using a pyranometer (Ji and Tsay, 2000) and the Pandora Spectrometer Instrument (Herman et al., 2009) at both sites. The combination

78 will be used to help validate three dimensional (3D) radiative transfer models applicable to analysis of
79 eclipse effects on radiances reflected back to space and reaching the Earth's surface. This study presents
80 the only calibrated spectral synoptic satellite data of the sunlit Earth ever obtained during an eclipse,
81 which should place tighter limits on validating radiative transfer studies under realistic conditions. The
82 data includes EPIC measured ozone absorption (316±5 DU Casper and 305±5 DU for Columbia, see Fig.
83 A3), O_2 A- and B-band absorption, clouds, aerosols, and scene and surface reflectivity (Herman et al.,
84 2018; Marshak et al., 2018).

85   DSCOVR observations of the entire sunlit Earth from the eclipse day, 21 August 2017, are compared
86 to those from two non-eclipse days to quantify the change of the global integral of reflected solar
87 radiation caused by the eclipse. We present a potential validation test data set for the 21 August 2017
88 eclipse for 3D radiative transfer models, namely the ratio of radiances without the eclipse on 20 and 23
89 August to the same regions that contained totality on 21 August 2017 (based on a suggestion in the
90 paper by Emde and Mayer, 2007).
91

Fig. 1 Synoptic view of the sunlit Earth perturbed by the 21 August 2017 total eclipse centered over Casper, Wyoming at 17:44:50 UTC. The black region is the eclipse umbra centered over Casper, WY. The color image has been adjusted from the images on https://epic.gsfc.nasa.gov/ by increasing the gamma correction to bring out the region of totality and surrounding clouds.

92

Columbia, MO

Fig. 02 Synoptic view of the total eclipse centered over Columbia, Missouri at 18:14:50 UTC. The black region is the eclipse umbra centered over Casper, WY. The color image has been adjusted from the images on https://epic.gsfc.nasa.gov/ by increasing the gamma correction to bring out the region of totality and surrounding clouds.

Section 2 describes the DSCOVR/EPIC instrument, available data, and monochromatic images based on measured counts per second, C/s. Section 3.1 presents a comparison between eclipse and non-eclipse days. Section 3.2 gives an estimate of the global reduction of reflected sunlight during the eclipse over Casper, WY and Columbia, MO.

2.0 EPIC Instrument and Data Description

The EPIC instrument onboard the DSCOVR spacecraft, in a six-month orbit near the L_1 point since June 2015, observed the Moon's shadow for about 3 hours. The EPIC data comprises a set of seven observations (16:44 to 19:44 UTC) starting in the Pacific Ocean and ending in the Atlantic Ocean, while synoptically observing the entire sunlit disk of the Earth (nominal size 0.5^O). EPIC is a 10 wavelength filter camera with a 2048x2048 pixel CCD (charge couple detector) using a 30-cm aperture Cassegrain telescope with a field of view (FOV) of 0.62^O that continuously points at the sunlit Earth. The sampling size on the Earth is nominally 8 km at the center of the image with an effective spatial resolution of $10x10$ km^2 for the 443 nm channel and $17x17$ km^2 for the remaining 9 filter channels. Operation of EPIC consists of sequentially selecting a filter from 2 rotatable filter wheels and an exposure time using a rotating disk shutter mechanism. Invariant exposure times were set at the beginning of the on-orbit

110   mission to fill the CCD wells to about 80 % and avoid blooming (a saturated pixel affecting its neighbors).
111   The CCD was calibrated for the sensitivity differences between the pixels (flatfielding), and
112   measurements were made in the laboratory and in-flight to obtain corrections for stray light effects.
113   Corrections for dark current are applied based on periodic measurements with the shutter closed. EPIC
114   is kept centered on the Earth during its 6-month north-south tilted Lissajous orbit about the Earth-Sun L_1
115   point. The spacecraft is never closer than 4° from the Earth-Sun line, which makes it possible to observe
116   an eclipse without the Moon being in the FOV. On 21 August 2017, DSCOVR was 7.7^O from the Earth-Sun
117   line. A more detailed description of EPIC is given in Herman et al. (2018) and Marshak et al., (2018).

118   The geolocated EPIC data (Counts per second, C/s) from each set of 10 wavelengths are
119   contained in an HDF5 formatted file available from the permanent NASA Langley data repository center
120   (https://eosweb.larc.nasa.gov/project/dscovr/dscovr_epic_l1b). Contained in each Level-2 data HDF5
121   file are the 2048 x 2048 array of C/s measured by EPIC and a common latitude and longitude grid. The
122   geolocated data are organized corresponding to the rectangular CCD grid, 1 data point per CCD pixel.
123   For the time of the eclipse, the illuminated CCD pixels are within a circular boundary corresponding to
124   Np = 2.59×10^6 illuminated pixels (illuminated pixels formed a circle of 1816 pixels in diameter out of a
125   maximum of 2048 pixels. To reduce the volume of telemetry data, all measurements, except those from
126   the 443 nm channel, were 2x2 averaged onboard DSCOVR to 1024 x 1024 pixels. After geolocation onto
127   a common latitude x longitude grid, the data from all channels are presented as 2048 x 2048 points with
128   off-earth points represented as a fill value "infinity". All of the data products (e.g., ozone amounts) are
129   also available at the above repository center.

130   The EPIC file names from the NASA data repository are interpreted as Year 2017, Month 08, Day
131   21, UTC 17:44:50, Version 2, which is 11:44:50 local daylight savings time in Casper, Wyoming. The
132   filename time refers to approximately the middle of the measurement sequence. Totality in Casper
133   started at 11:42:39 and ended at 11:45:05. Version 2 refers to the reprocessing of data with the latest
134   CCD flat-fielding and stray-light corrections (Herman et al., 2017; Marshak et al., 2017; Geogdzhayev and
135   Marshak, 2017), and the geolocation algorithms.

136   The observing conditions for 21 August 2017 ranged from significant cloud cover over the oceans to
137   nearly clear skies over the United States (Figs. 1 and 2). The synoptic observations provided a unique
138   opportunity to estimate the fraction of reduced reflected radiation from the entire sunlit Earth caused
139   by a total solar eclipse. Two of the synoptic observations were timed so that they centered on Casper,
140   Wyoming (42.8666° N, 106.3131° W, 17:44:50 UTC) and Columbia, Missouri (38.9517° N, 92.3341° W,
141   18:14:50 UTC). Ten narrowband images were obtained at center vacuum wavelengths λ_i of 317.5±0.5,
142   325±0.5, 340±1.3, 388±1.3, 443±1.3, 551±1.5, 680±0.8, 688±0.42, 764±0.5 and 779.5±0.9 nm (Herman
143   et al., 2018). Of these, 388, 443, 552, 680, and 779 nm radiances are not strongly absorbed in the
144   atmosphere and are used for estimating the reduction in reflected radiances from the Earth. The others
145   are strongly affected either by ozone (317, 325, 340 nm) or oxygen absorption (688, 764 nm) in the
146   atmosphere, but give similar radiance percent reductions during the eclipse compared to non-absorbed
147   channels.

148   The non-absorbed wavelength observations were combined to produce eye-realistic color images
149   (https://epic.gsfc.nasa.gov). For this eclipse day study, 21 August, the original color images were
150   modified by increasing the gamma correction to better show the umbra over Casper, Wyoming and
151   Columbia, Missouri (Figs. 1 and 2 based on a suggestion by Steven Albers and Michael Boccara, 2017,
152   Private Communication). The images include Rayleigh scattering effects that cause light from the
153   penumbral region to increase illumination within the umbra along with scattering from clouds and
154   aerosols.

155   Table 1 summarizes eclipse timing and location details for Casper, Wyoming. During the 2.7
156   minutes needed to obtain the five listed wavelength channel images, the center of totality moves at
157   about 46 km/minute or covering approximately 124 km. Based on the image in Fig. 1, the entire
158   measurement took place within the observed nearly clear-sky region surrounding Casper, Wyoming. A
159   similar table could be constructed for the eclipse totality region near Columbia, Missouri.

Table 1 *Eclipse Measurement Timing and Location Details for 5 Wavelengths*
Eclipse Maximum and EPIC Image Times. Total Measurement Duration 2.7 minutes

Wavelength (nm)	Date and Time	Location Name	Longitude
	2017-08-21 17:35:40	Eclipse West Edge of WY state	$-111^{o}02'$
551	2017-08-21 17:42:36	West of Casper	$-106^{o}22'$
680	2017-08-21 17:43:30	West of Casper	$-106^{o}21'$
Casper Wyoming	2017-08-21 17:43:51	Casper WY	$-106^{o}19'$
780	2017-08-21 17:44:24	Near Glenrock WY	$-105^{o}52'$
443	2017-08-21 17:44:50	West of Douglas WY	$-105^{o}14'$
388	2017-08-21 17:45:18	West of Douglas WY	$-105^{o}17'$
	2017-08-21 17:48:04	Eclipse East Edge of WY state	$-104^{o}03'$

160

161   The timing and predicted shape of the Moon's shadow over Casper, Wyoming and Columbia,
162   Missouri can be seen at https://eclipse2017.nasa.gov/eclipse-maps. An annotated portion of the figures
163   for Casper and Columbia are reproduced in the Appendix (Fig. A1). The predicted totality shadow (Fig.
164   A1) over Casper was elliptical in shape with a width of about 116 km (about 1.5^{o} in latitude or
165   longitude). The similar drawing for Columbia, Missouri shows a more nearly circular region of totality.
166   The dimension of the partial eclipse for 90 % obscuration is about 5° in latitude or longitude. The region
167   of 75 % obscuration covers a latitude range 32° to 46° or about 1200 km. An obscuration region of this
168   size produces a significant decrease in the percentage of total solar irradiance reaching the Earth's
169   surface and in the amount reflected back to space. EPIC synoptically measures both the local and sunlit
170   portion of the global percent change in reflected radiance, which is approximately the same as the
171   percent change in global surface irradiance for the wavelength range from 388 to 780 nm. An exception
172   is within the umbral region, where the percent change is larger at the surface than at the top of the
173   atmosphere. The three wavelength channels shorter than 388 nm are affected by ozone absorption and
174   also do not contribute much to the sum of reflected radiances compared to the range from 388 to 780
175   nm. The energy content of 317 to 340 nm are not included in the quantitative estimate of broadband
176   (UV + visible) reduced reflected radiance, nor are the strongly absorbed O_2 A- and B-band channels, 688
177   and 764 nm, included. However, the effects of the eclipse on all 10 channels are individually estimated.
178

179   **2.1 Monochromatic Eclipse Images**

180

181   Before quantitatively examining the EPIC data from the eclipse in units of C/s or reflectance, the
182   same data can be represented as monochrome grey-scale images. The images (Fig. 3 with North down)
183   range from 340 nm, with strong Rayleigh scattering effects and some ozone absorption, to 780 nm in
184   the near infrared. North is selected as down to correspond to a 3D projection image presented later.
185   Because of the clarity of the atmosphere at 780 nm, the image serves as a geographic map of the Earth
186   as viewed by EPIC where North and South America are clearly visible.
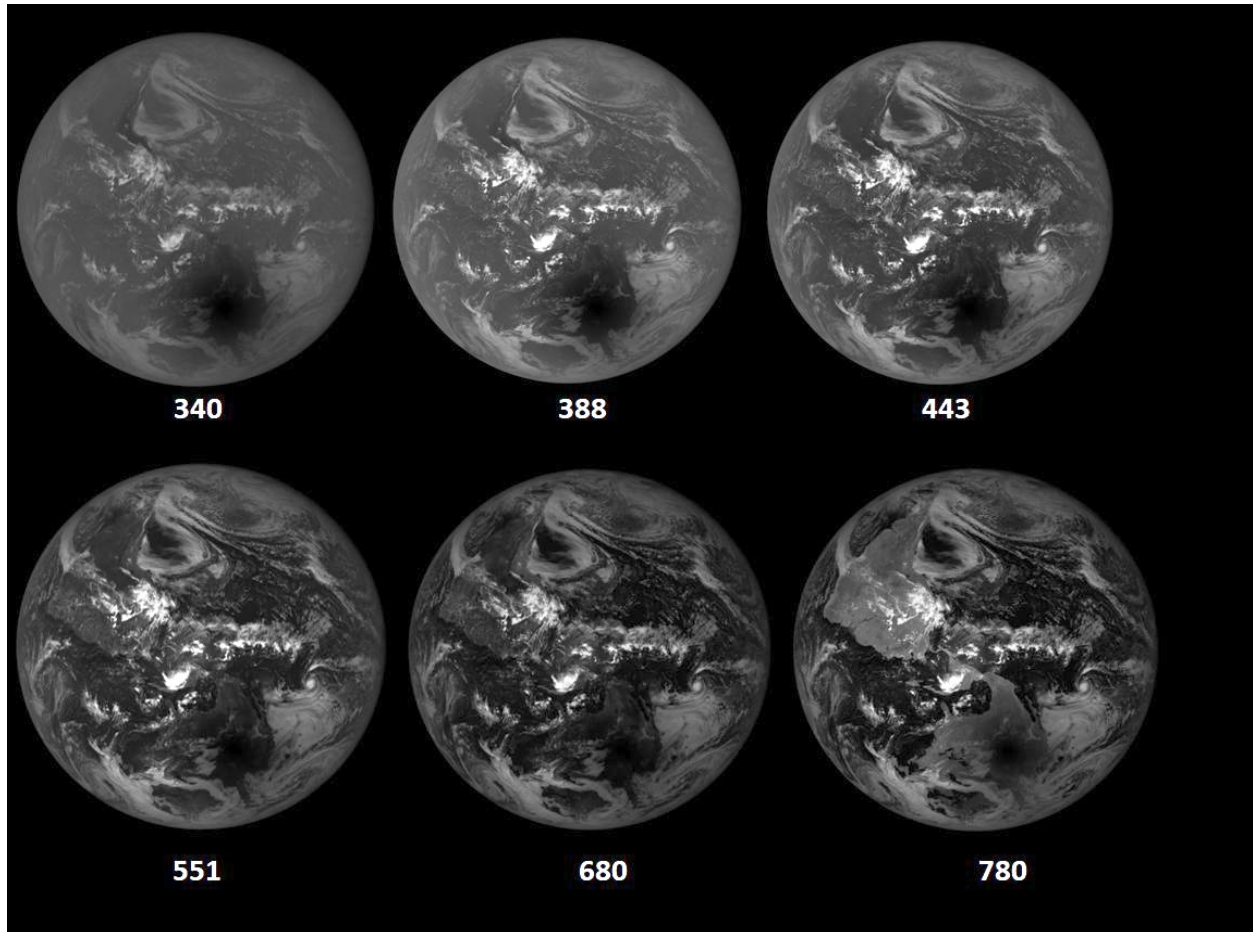
Fig. 3 Greyscale images for 6 of the DSCOVR/EPIC channels for the eclipse over Casper Wyoming showing the blurring caused by Rayleigh scattering and the dark land and ocean surfaces at 340 nm to the almost clear atmosphere and bright continental surfaces at 780 nm. The images were obtained over a period of 2.7 minutes. North is facing down.

187

188

189

190

191   **3.0 Results**

192   **3.1 Comparison of EPIC Observations of Eclipse Totality (21 Aug) with Non-Eclipse Days (20 and 23**
193   **Aug) for Casper, WY and Columbia, MO**

194   Atmospheric conditions during the eclipse at Casper, Wyoming were almost cloud-free
195   compared to Columbia, Missouri, which had optically thin low altitude clouds (Fig. 2). Figure 4 shows the
196   cloud cover on the day of the eclipse, 21 August 2017 (panel A) about 90 minutes before totality at
197   Casper and about 2 hours after totality. The images (north is up) show that the skies remained relatively
198   clear over the northern United States for the duration of the eclipse. A similar set of images (panel B)
199   are shown for the day before (20 August) and two days after the eclipse (23 August). There was no
200   useable data available on 22 August. Data obtained on 20 and 23 Aug. at approximately the same UTC
201   (backscatter phase angle for a given location on Earth) as occurred during the total eclipse are used as
202   reference data to compare with the eclipse data on 21 Aug. The basic global patterns of cloud cover are
203   similar for all three days, but not identical. As shown later, the amount of light reflected back to space is
204   approximately the same on the two non-eclipse days 20 August and 23 August.
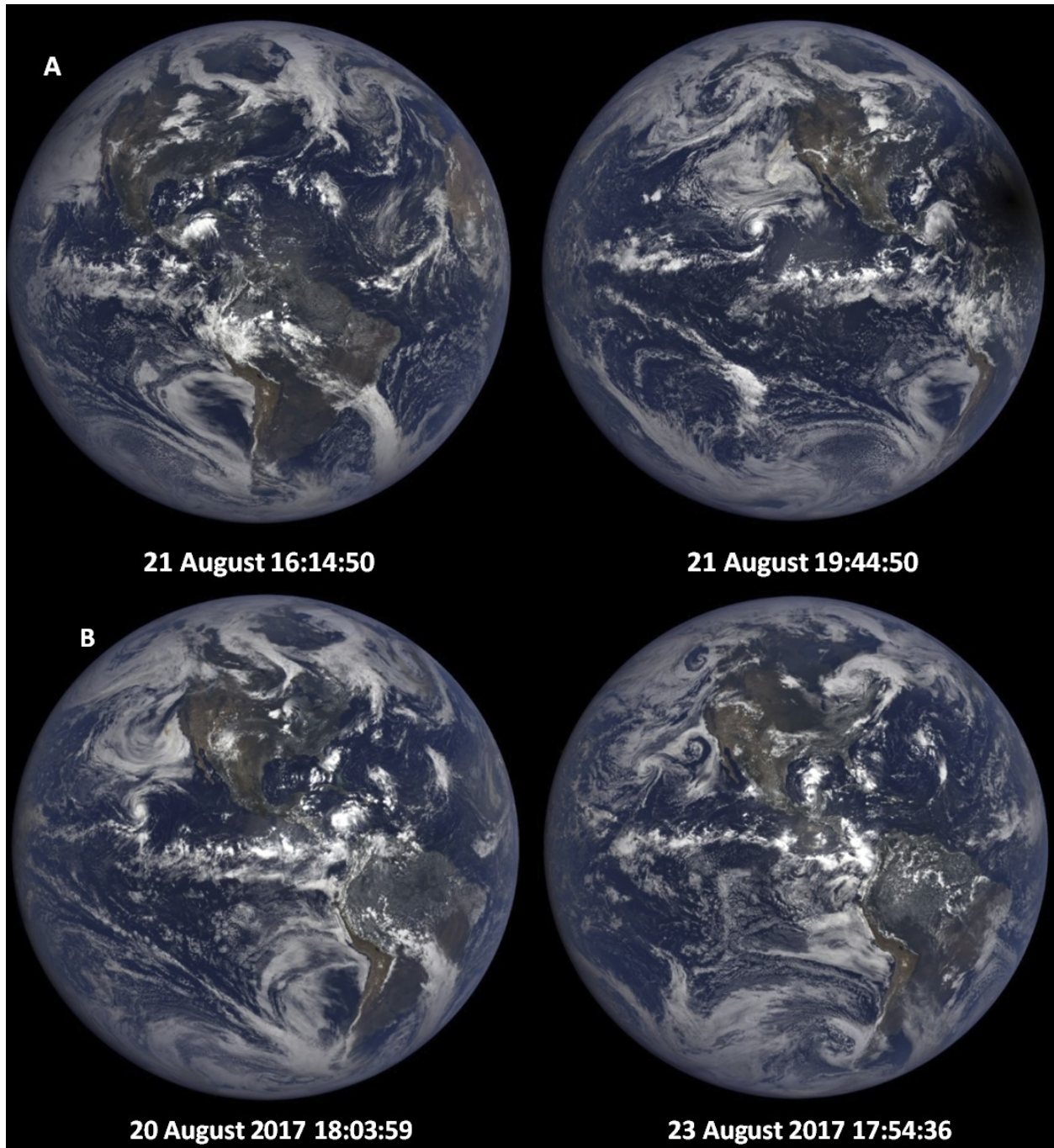
205

Fig. 4 Panel A: Synoptic natural color images on 21 August at 16:14 and 19:44 before and after the eclipse over the US, and Panel B: the days before and after the eclipse selected to be as close as possible to the phase angle (UTC 17:44:50) as the time of totality over Casper, Wyoming. North is facing up.

206

207   Figure 5 (upper panels A and B) shows longitudinal slices of 443 nm reflected solar radiances in
208   C/s towards L_1 through the locations corresponding to Casper, Wyoming and Columbia, Missouri at their
209   respective times of totality. The lower panels (C and D) of Fig. 5 show 443 nm measurements in C/s on
210   20 Aug at 18:04 UTC before the eclipse for nearly identical solar phase angles conditions for both sites.

211 The effect of clouds at the Columbia site compared to Casper can be seen in terms of the depth of the
212 umbra (Panels A: ratio = 1530 and B: ratio = 37) relative to the average C/s from -140° to -150°
213 longitude. Similarly, on the preceding day, 20 Aug (panels C and D), the cloud effect is small at Casper,
214 1.2×10^{4} C/s, compared to Columbia, 5×10^{4} C/s and just to the west of Columbia, 1.3×10^{5} C/s.
215
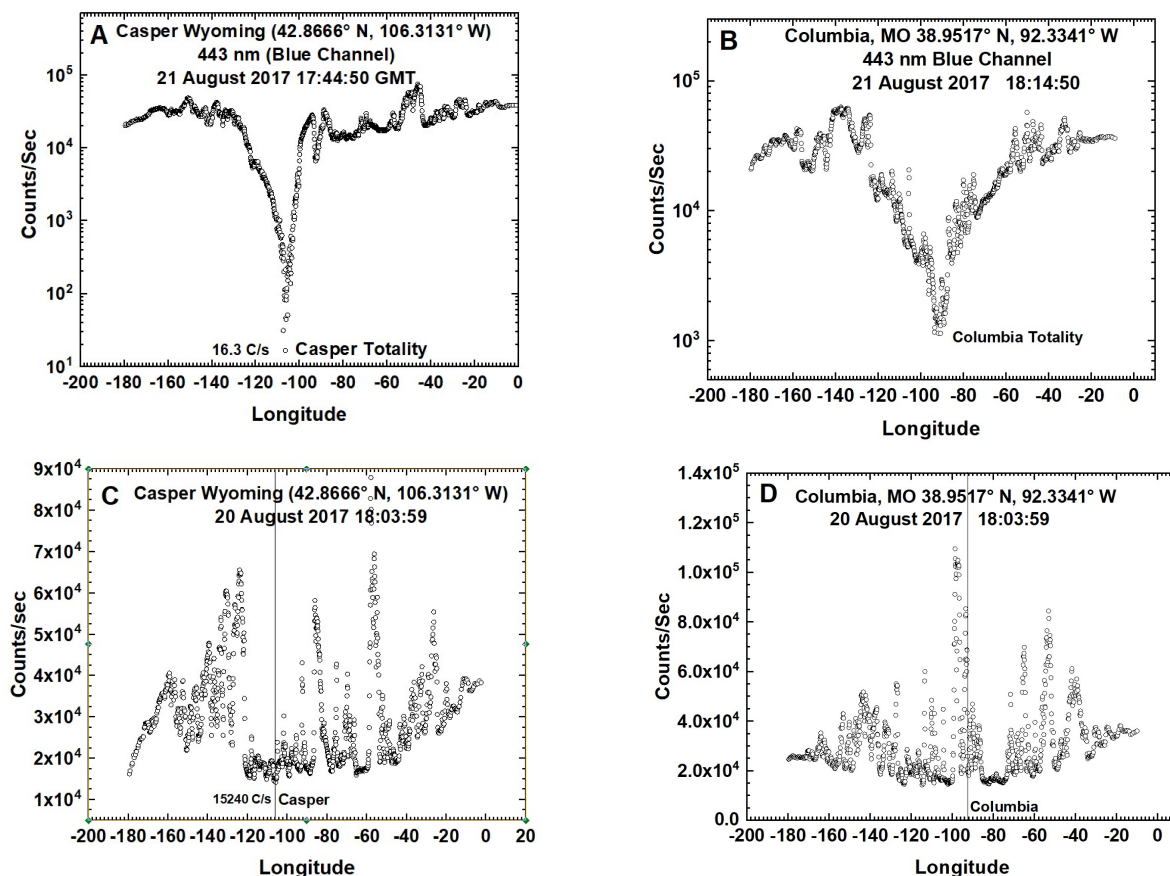
Fig. 5 Top: The effect of an eclipse (21 Aug) on the measured C/s reflected back to space as a function of
longitude (degrees) for two locations, Casper Wyoming (left) and Columbia Missouri (right). Bottom:
Measured C/s reflected back to space on 20 Aug. A $\log_{10}$ scale is used to show details of the spatial
variability mostly caused by clouds.

216

217   The minimum 443 nm values during totality are 16.6 C/s for Casper and 312 C/s for Columbia.
218 On 20 Aug. EPIC measured 15240 C/s and 52728 C/s, respectively, showing the effect of increased
219 cloudiness for Columbia. While Fig. 5 is expressed in C/s, the data can be converted to radiance W/(m^{2}
220 nm sr) based on an in-flight determined radiance calibration coefficient of $K_R(443nm) = 5.291 \times 10^{-6}$
221 W/(m^{2} nm sr C/s) (Geogdzhayev and Marshak, 2017; Marshak et al., 2018; Herman et al. 2018). For 443
222 nm channel, an average count rate for the illuminated earth is 3×10^{4} C/s corresponding to a radiance of
223 0.159 W/(m^{2} nm sr). EPIC calibration constants for 8 of the 10 channels were obtained by in-flight
224 comparisons of reflectance measured by two well calibrated low Earth orbiting satellite instruments,
225 OMPS (Ozone Mapping Profiler Suite for UV channels) and MODIS (Moderate Resolution Imaging
226 Spectroradiometer for visible and near-IR channels) for simultaneously viewed Earth areas with the

227 same satellite view and solar zenith angles (Herman et al., 2018; Geogdzhayev and Marshak, 2017). The
228 O_2 A- and B-band channels were calibrated using lunar data when the Moon was within the field of view
229 of EPIC. Detailed discussions and values of all EPIC calibration coefficients $K(\lambda)$ are given by Geogdzhayev
230 and Marshak (2017), Herman et al, (2018) and Marshak et al., (2018). Most of the conclusions in this
231 study are in terms of ratios of C/s from the same wavelength channel at approximately the same solar
232 phase angle that are independent of the absolute calibration conversion from C/s to radiance.
233
234 The ratio $R_{EN}(\lambda_i)$ = I(20 August)/I(21 August) is used to characterize the eclipse effects at the top
235 of the atmosphere. Because the solar phase angles are nearly the same, the effects of the 172°
236 backscatter angle ("hot spot" caused mostly by minimized shadows) and ocean specular reflection are
237 also nearly the same on both days.

238 There is considerable variability in $R_{EN}(\lambda_i)$ = I(20 August)/I(21 August) as a function of wavelength
239 that is partially caused by the 2.7 minutes needed to obtain measurements for all 10 wavelengths.
240 During the 2.7 minutes, the center of totality moved about 124 km or about 1.7^O longitude, meaning
241 that the ratio was affected by atmospheric variability (mostly cloud effects) in the successive scenes
242 containing the eclipse totality for each wavelength. The ratios $R_{EN}(\lambda_i)$ of C/s on the eclipse day to the
243 preceding non-eclipse day are shown in Fig. 6 for all 10 wavelength λ_i channels and two sites (Casper, Fig
244 6a and Columbia, Fig. 6b) and summarized in Table 2. The same reference data from 20 Aug is used for
245 both sites, since it was the closest in UTC for both the Casper and Columbia eclipse times.

246

247 *Table 2 Maximum Radiance Ratio $R_{EN}(\lambda_i)$ during eclipse totality 17:44:50*
248 *UTC (Casper) and 18:14:50 UTC (Columbia) compared to 20 Aug. at*
18:03:59 for both sites (see Fig. 6).

| Wavelength λ_i (nm)	Max. $R_{EN}(\lambda_i)$ C/s Casper, Wyoming	Max. $R_{EN}(\lambda_i)$ C/s Columbia, Missouri
317.5	255	50
325	245	49
340	475	59
388	3500	81
443	935	169
551	5455	183
680	220	171
688	365	246
764	302	92
780	395	38
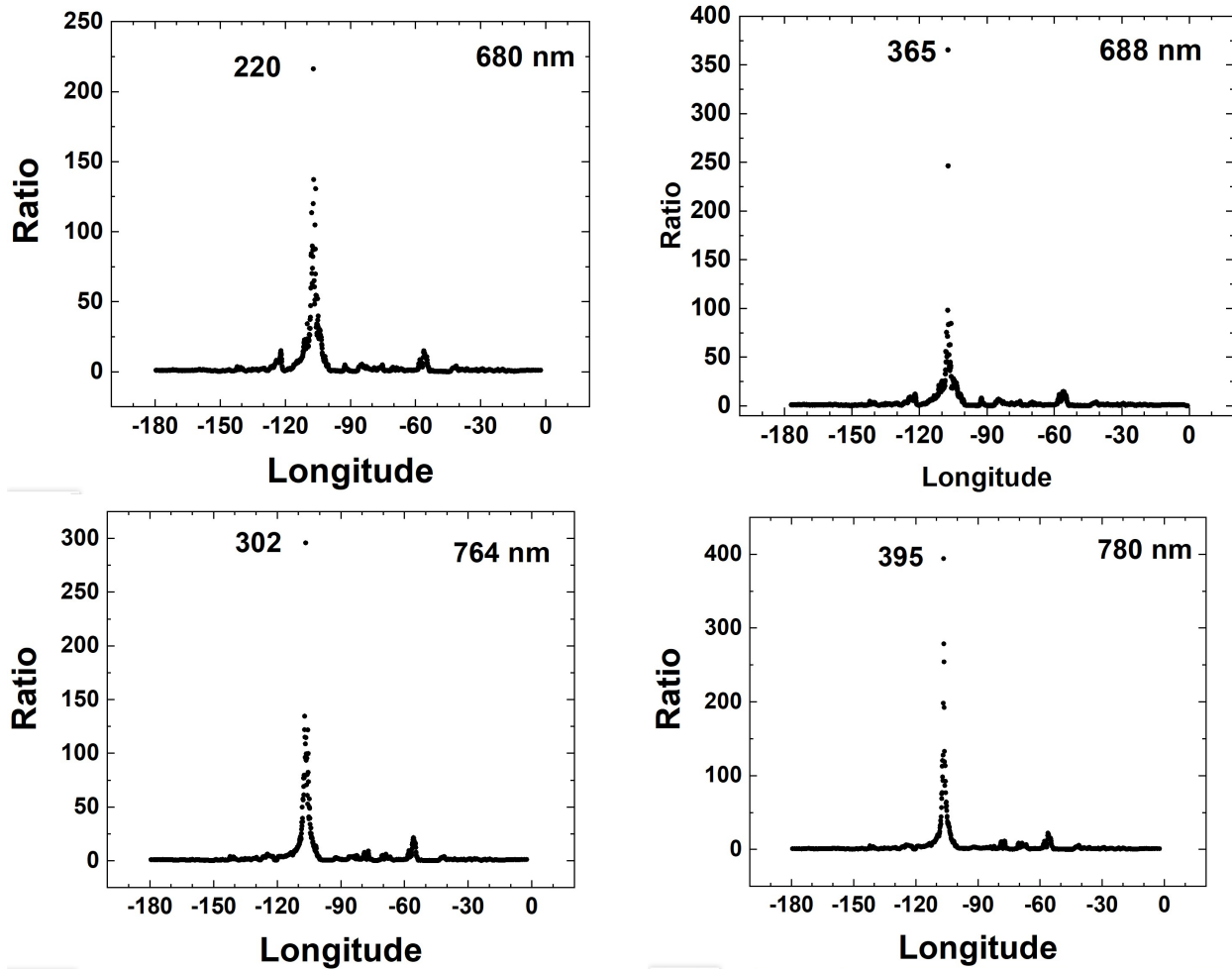
Fig. 6a. The ratio $R_{EN}(\lambda_i)$ = I(Aug20)/I(Aug21) at the time of the Eclipse in Casper Wyoming for wavelengths 317.5 to 780 nm. The channels 317.5 to 240 nm are affected by ozone absorption and the channels 688 and 764 nm are within the O_2 B and A absorption bands.
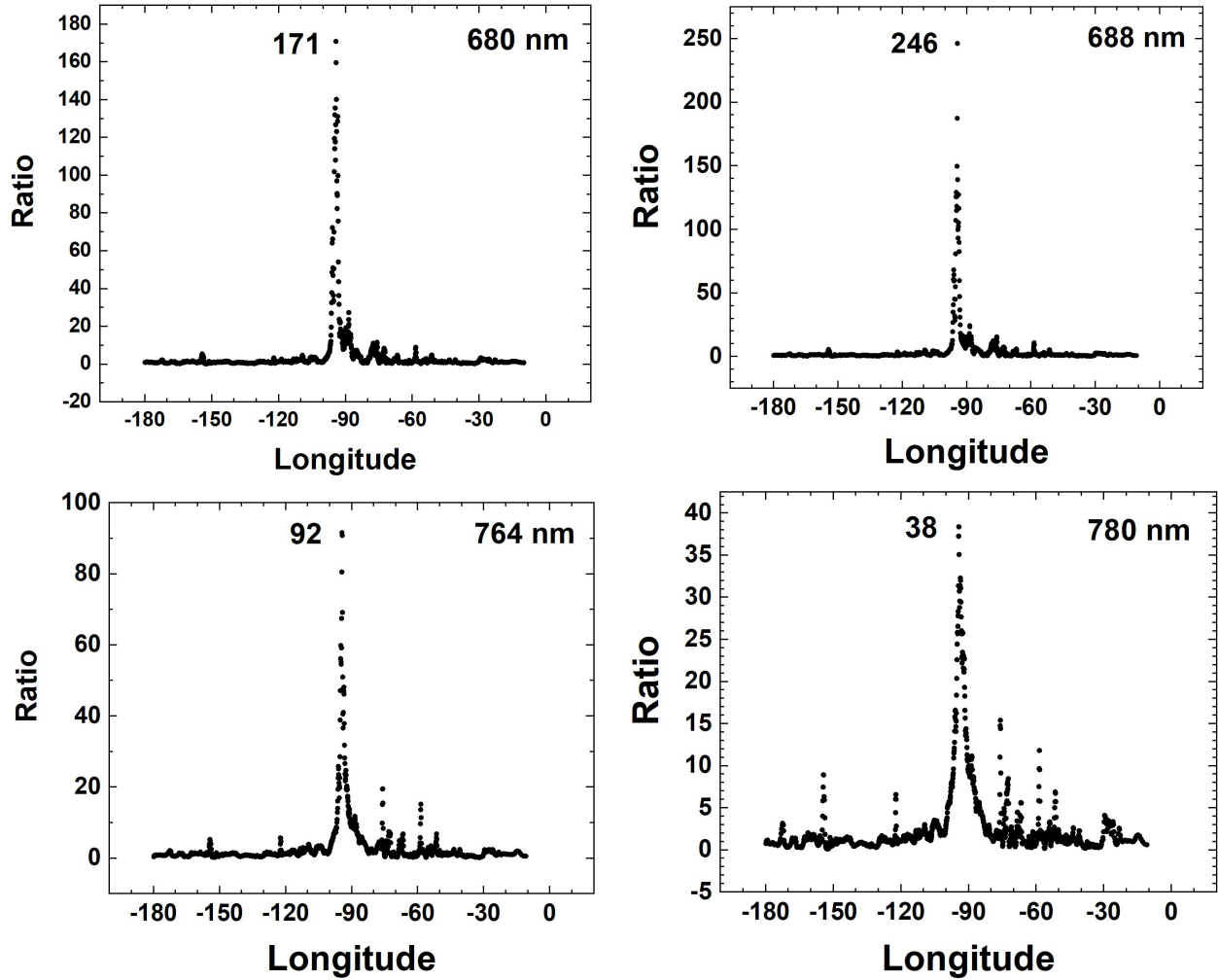
252

253
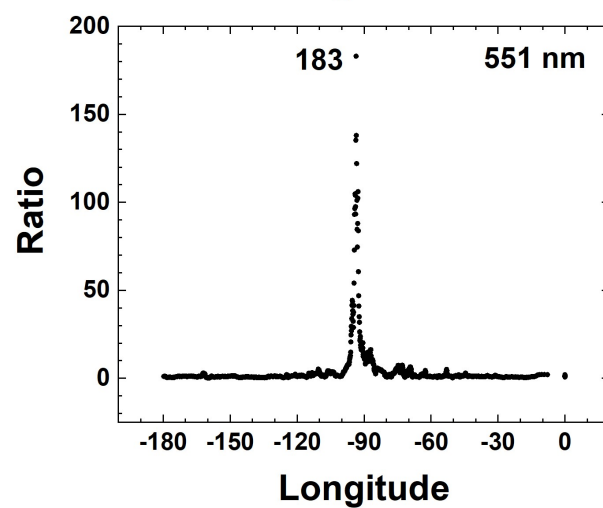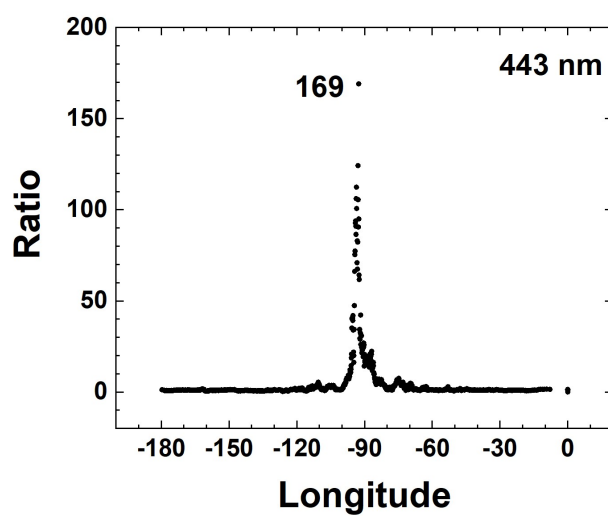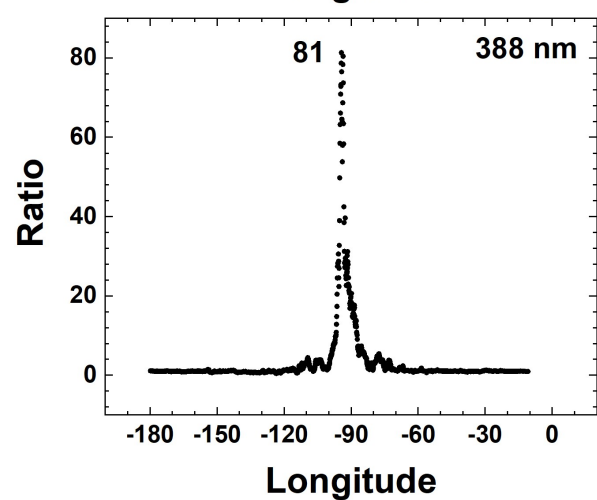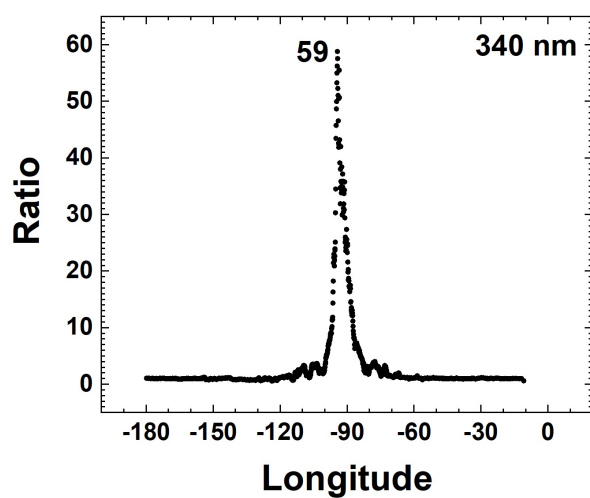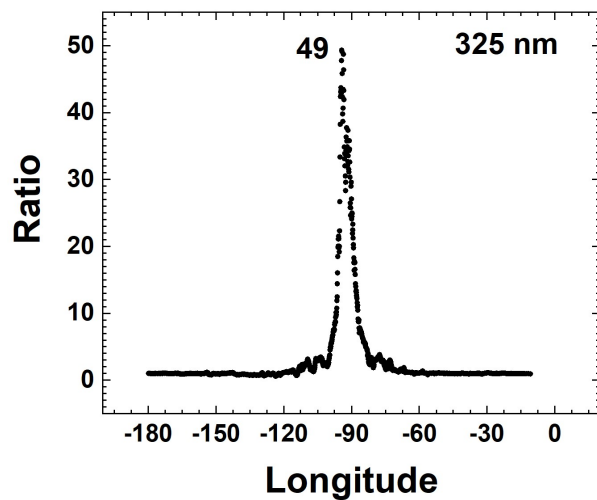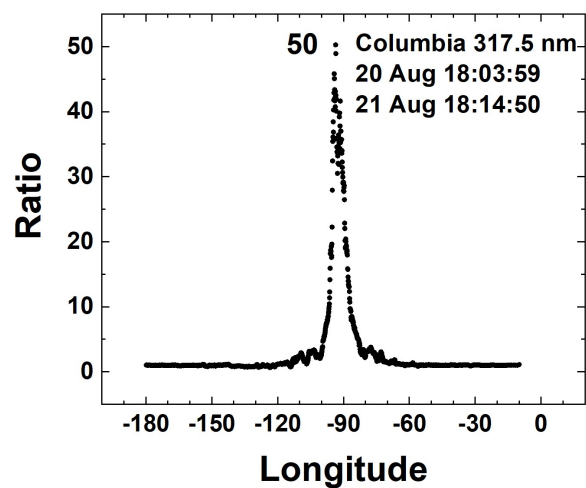
13

Columbia 317.5 nm
20 Aug 18:03:59
21 Aug 18:14:50

254

Fig. 6b. The ratio $R_{EN}(\lambda_i) = I(Aug20)/I(Aug21)$ at the time of the Eclipse in Columbia, Missouri for wavelengths 317.5 to 780 nm. The channels 317.5 to 340 nm are affected by ozone absorption and the channels 688 and 764 nm are within the O_2 B and A absorption bands.

255

256   For the eclipse study, the range of synoptically observed longitudes is approximately from the
257 international dateline (-180°) to almost longitude of Greenwich, England (0°). The nearly clear-sky in
258 Casper with optically thin high cirrus clouds permits the reflected light during totality to become very
259 small (about 17 C/s for 443 nm compared to 1.5×10^4 C/s on 20 August at the same longitude). Columbia
260 had more low altitude cloud cover than Casper (Fig. 2) with the cloud cover extending into the region of
261 totality. The effect of this cloud cover can be seen in Fig. 6, where the maximum $R_{EN}(443, Columbia) =$
262 169 compared to 935 for Casper. Table 2 provides the eclipse radiance ratio $R_{EN}(\lambda_i)$ for the five non-
263 absorbed wavelength and 5-absorbed channels that can help validate 3D radiative transfer models. The
264 measured lower values $R_{EN}(\lambda_i)$ at Columbia compared to Casper show that there is high sensitivity in the
265 TOA upwelling measured ratios to the presence of even optically thin clouds. A detailed radiative
266 transfer study for realistic conditions is made feasible by using EPIC's simultaneous estimates of cloud
267 reflectivity and transmission, cloud height, ozone amounts, (Fig. A3 and Herman et al., 2018), and

268   aerosol amounts (Torres et al., 2018 private communication).   These data products are available from
269   the NASA-Langley data repository referenced above.

270
271   **3.2 Global reduction of reflected sunlight during the eclipse over Casper WY**

272

273   The unique DSCOVR/EPIC measurements provide estimates of the fractional reduction of
274   sunlight from 388 to 780 nm reflected back to space for the entire sunlit globe caused by the eclipse
275   shadow on the Earth. To do this, all of the light reaching EPIC in each of the five non-absorbed channels,
276   388, 443, 551, 680, and 780 nm, are integrated over the visible sunlit Earth and compared (percent
277   difference $PD(\lambda_i)$) with a nearly identical viewing geometry (nearly the same UTC) from the previous and
278   next days. The assumption is that the major cloud features change slowly on a global scale over
279   relatively short periods (Figs. 1 to 3). A test of this hypothesis is that the PD between successive non-
280   eclipse days is small compared to the eclipse day $PD(\lambda_i)$ with a non-eclipse day.

281   In the 3D Fig. 7 for 443 nm, the nearly cloud free eclipse region is the blue area in the midst of
282   greens, yellows, and reds. The high red values correspond to fairly reflective clouds mostly seen near
283   the equator (Fig. 1). The yellows and greens correspond to lower altitude clouds that tend to have
284   smaller reflectivities. Integrating over all of the pixels for the eclipse on 21 August 2017, using the file
285   named epic_1b_20170821174450_02.h5, we get S(DOY, UTC) = 5.34366×10^{10} C/s for DOY=233 (21
286   August 2017) and UTC=17:44:50. For the eclipse day, the 443 nm average C/s = 2.0631×10^{4}, which
287   corresponds to 2.0631×10^{4} K_R(443 nm) = 0.11 W/(m^2 nm sr).   Peak values are approximately 1×10^{5} C/s,
288   or about 0.53 W/(m^2 nm sr). Figure 7 is oriented with north down so as to be able to see into the eclipse
289   shadow region. A similar figure is obtained for Columbia, Missouri with reduced depth caused by some
290   visible light cloud cover extending into the region of totality.
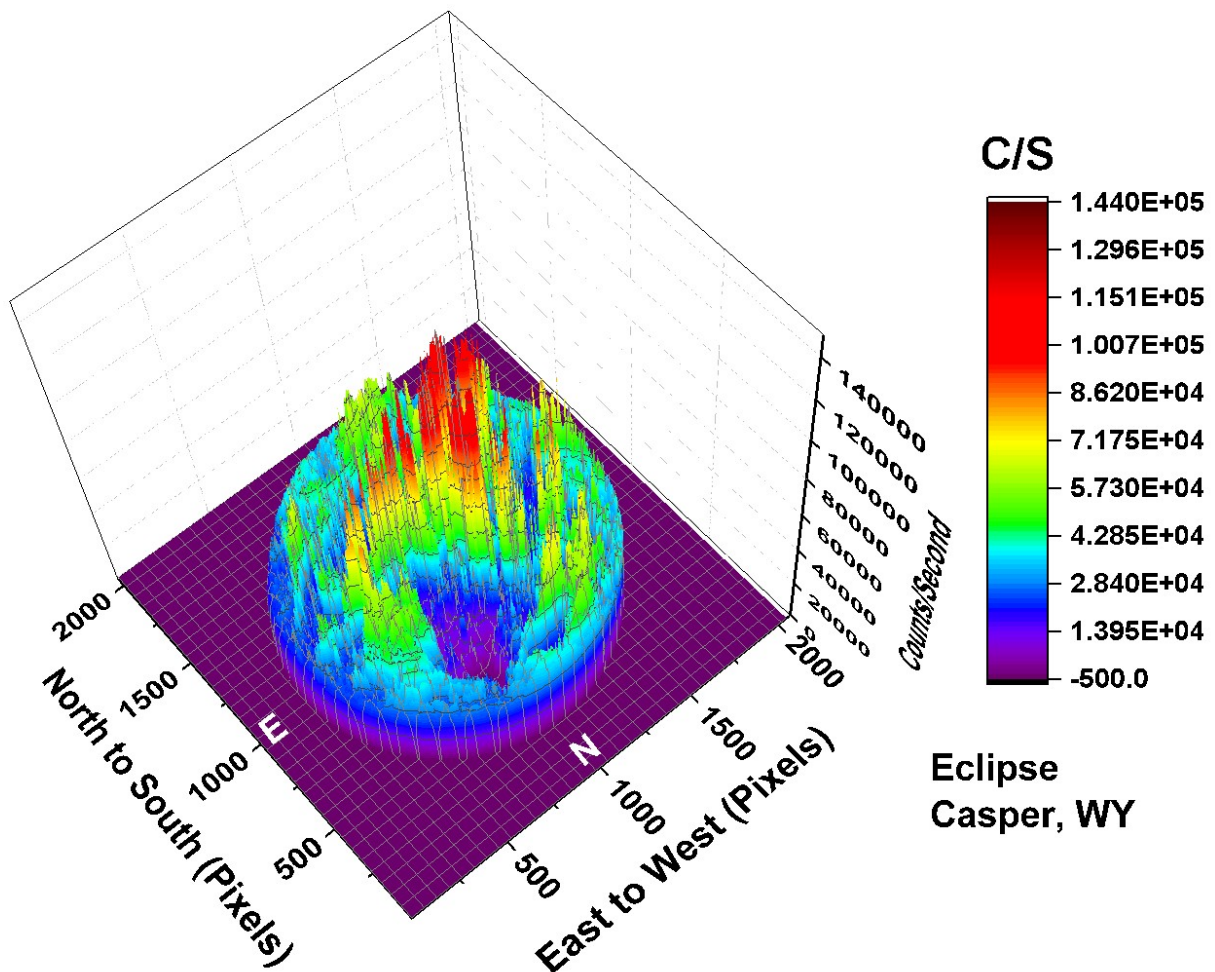
291

Fig. 7 The C/s observed by EPIC for the 443 nm channel corresponding to the color image shown in Fig. 1. In the data file, the fill-word infinity has been replaced by the number zero. In this image there are approximately Np = 2.59x10^6 illuminated pixels out of 2048^2 = 4.194304x10^6 pixels (61.8 %).

292

293   Measured C/s images for six wavelength channels (340 to 780 nm) on 20, 21, and 23 August (Fig.
294   8) were selected to be as close as possible to the UTC time of the eclipse in Casper Wyoming, keeping
295   the scattering phase angles nearly constant. Similar images for the strongly absorbed channels 317.5,
296   325, 688, 764 nm channels are shown in the appendix (Fig. A2). The middle images in panels B and E of
297   Figs. 8a, 8b and 8c are for the eclipse over Casper, Wyoming. These images are in the same format as
298   Fig. 3, but rotated with north up. Unlike Fig. 3, The scale in Fig. 8 was selected so that the brightest
299   clouds do not saturate the image. The increase in scale makes the land surfaces less visible. While the
300   figures are similar from wavelength to wavelength, there are differences in the depth of the eclipse
301   totality and the reflectivities of the surrounding clouds. In general, the equatorial clouds with higher C/s
302   (reflectivities) tend to reach higher altitudes. This is confirmed by examining the C/s in the strongly
303   absorbed O$_2$ A-band channel (Fig. A2b and Herman et al., 2018).

304
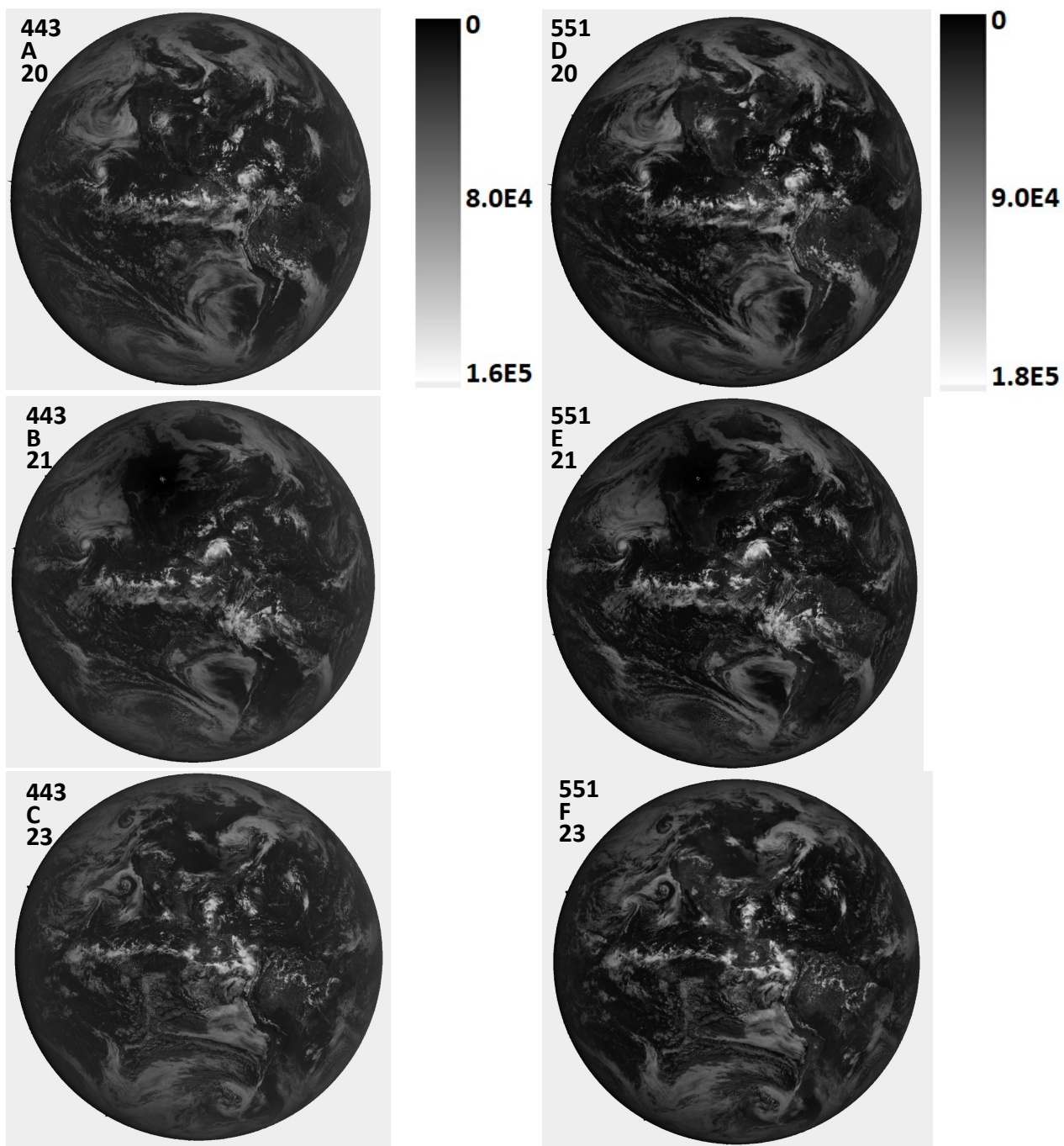
Figure 8a Image in C/s for 443 and 551 nm for 20 Aug.(A+C), 21 Aug. (B+E), and 23 Aug. (C+F). The scale applies to the specific wavelength. North is up.

305

306
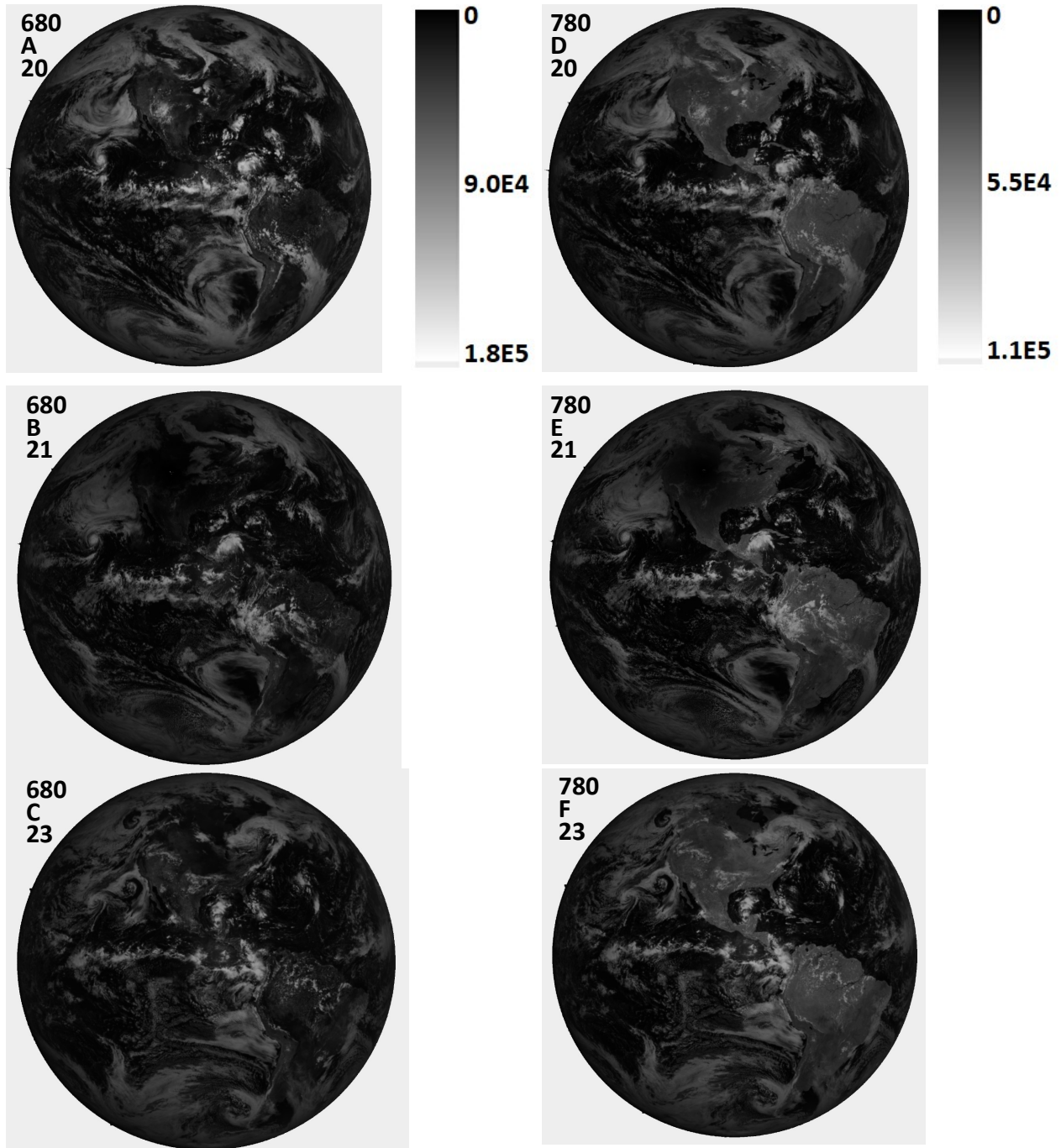
Figure 8b Image in C/s for 680 and 780 nm for 20 Aug.(A+C), 21 Aug. (B+E), and 23 Aug. (C+F). The scale applies to the specific wavelength. North is up.

307

308   EPIC measured $C(\lambda)$ in C/s for each pixel can be converted to Earth top of the atmosphere
309 reflectance $Re(\lambda)$ using the in-flight derived calibration coefficients $K(\lambda)$, where $Re(\lambda) = K(\lambda)\ C(\lambda)$. For
310 the six wavelength channels in Fig. 8 plus the O_2 A- and B-band channels, $K(340) = 1.975 \times 10^{-05}$, $K(388) =$
311 2.685×10^{-05}, $K(443) = 8.340 \times 10^{-06}$, $K(551) = 6.66 \times 10^{-06}$, $K(680) = 9.30 \times 10^{-06}$, $K(687.75) = 2.02 \times 10^{-05}$, $K(764)$
312 $= 2.36 \times 10^{-05}$, and $K(780) = 1.435 \times 10^{-05}$ (Herman et al., 2018; Geogdzhayev and Marshak, 2018; Marshak

313 et al., 2018). To estimate the percent reduction in outgoing radiances, the ratios of integrals over the
314 illuminated CCD for each wavelength channel are formed for nearly the same Earth geometry on days
315 preceding and following the eclipse. Either the integrated reflectances or the integrated C/s x 10^{-7} (Eqn.
316 1) for Tables 3A for Casper, Wyoming and 3B for Columbia Missouri) over the CCD pixels, ICs(λ), can be
317 used directly, since they are linearly proportional to the integral of the photons received by the
318 illuminated pixels.
319
320   Table 3 and Fig. 9 show that the global reduction of backscattered light caused by the eclipse is
321 similar for the two sites even though there is more cloud cover locally over Columbia than Casper. This is
322 because only 30 minutes have elapsed between the two measurements, which is not enough time for
323 the global cloud cover to have significantly changed.
324

Table 3A Global integral of reflected light ICs for the UTC of the Casper, WY eclipse on 21 August and for
the closest solar phase angle from 20 and 23 August. PD is the percent difference caused by the eclipse.
Units are ICs x 10^{-7}

λ_i (nm)	20 August 2017 16:58:31 UTC	21 August 2017 17:44:50	23 August 2017 17:54:36	Avg. PD
317.5	280.5	258.8	282.0	9±0.3
325	460.6	425.5	464.2	9±0.4
340	3183	2946	3213	9±0.5
388	2034	1878	2044	9±0.3
443	5808	5344	5813.2	9±0.05
551	5619	5078	5573	10±0.5
680	3790	3433	3773	10±0.3
688	1129	1010	1110	11±0.9
764	671.9	585.9	651.9	13±1.7
780	2794	2491	2799	12±0.1

325

Table 3B Global integral of reflected light ICs for the UTC of the Columbia, MO eclipse on 21 August and
for the closest solar phase angle from 20 and 23 August. PD is the percent difference caused by the
eclipse. Units are ICs x 10^{-7}

λ_i (nm)	20 August 2017 18:03:359 GMT	21 August 2017 18:14:50	23 August 2017 17:54:36	Avg. PD
317.5	281.3	258.3	282.0	9±0.1
325	461.6	425.9	464.2	9±0.3
340	3193	2956	3213	8±0.3
388	2034	1884	2044	8±0.3
443	5813.7	5372.3	5813.2	8±0.01
551	5586	5091	5573	10±0.1
680	3790	3453	3773	10±0.2
688	1121	1011	1110	10±0.5
764	661.2	576.0	651.9	14±0.8
780	2794	2475	2799	13±0.1

326

327   Figure 9 shows a plot of the data contained in Table 3 based on Eqn. 1. The two non-eclipse days are
328   nearly identical, while the eclipse day (21 Aug) is significantly lower at all wavelengths. The
329   backscattered light (in C/s) peaks near 500 nm and then decreases toward longer wavelengths, since
330     $C(\lambda)$ is proportional to the solar irradiance, which decreases with λ after approximately 550 nm.

$$ICs(\lambda) = \int_0^{2048} \int_0^{2048} C(\lambda, x, y)dxdy \tag{1}$$

over Np = 2.59×10^6 illuminated pixels on 20, 21, 23 August 2017

331
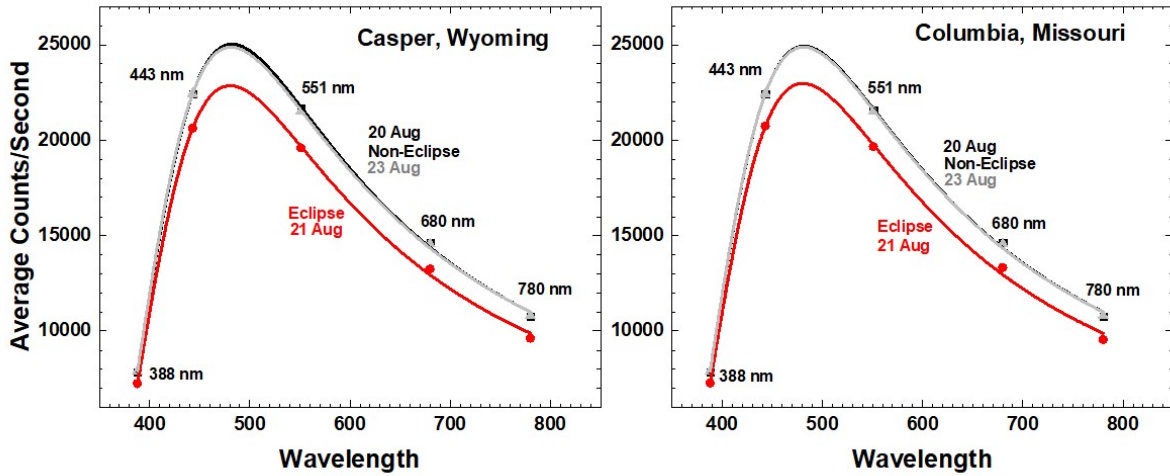
Fig. 9 Average $(ICs(\lambda)/Np)$ reflected light in C/s for eclipse (21 Aug. red) and non-eclipse (20 Aug. and 23 Aug. (black and grey) days from Table 3 and Eqn. 1 for Casper and Columbia. The exact locations of the maxima are from curve fitting to the discrete wavelength measurements.

332

333   For the 443 nm channel, the result is an approximate decrease of 9 % on 21 August at 11:44:50
334   for Casper and 8% at 12:14:50 for Columbia local time. As a reference, we compare two non-eclipse
335   days (19 and 23 August). The relative difference is (5808-5813)/5813 0.1 % for Casper and 0.01 % for
336   Columbia, which is much smaller than the 9 % decrease produced by the eclipse on 21 August. The
337   comparison of the 443 nm eclipse day with two non-eclipse days gives a measure of the uncertainty in
338   the calculation (e.g., 9 ± 0.05 % for Casper and 8 ± 0.01% for Columbia).

339

340   Percent difference $PD(\lambda_i)$ calculations for λ_i = 317.5, 325, 340, 388, 443, 551, 680, 688, 764, and
341   780 nm, based on Eqn. 1 are summarized in Table 3A, yielding $PD(\lambda_i)$ = 9, 9, 9, 9, 9, 9, 10, 10, 13, and 12
342   % reductions in backscattered radiances in the direction of L_1, respectively for Casper with similar values
343   for Columbia. The PD(764) within the strongly absorbing O_2 A-band is 13 % for Casper and 14% for
344   Columbia, even though the reflected ICs(764) is much lower than the surrounding non-absorbed bands.
345     $PD(\lambda_i)$ is smaller at shorter wavelengths because of increased Rayleigh scattering that reduces the
346   contrast of the Moon's shadow by scattering light into the umbra and penumbra regions from the areas
347   adjacent to the total and partial eclipse. The fact that adjacent absorbed and non-absorbed wavelengths

21

348 give consistent PD(λ_i) suggests that most of the effect comes from clouds and Rayleigh scattering and
349 not from the relatively low reflectivity surface where the amount of clear-sky penetrating radiances are
350 small for 688 and 764 nm channels.

351

352   The TOA eclipse measurements made by EPIC are near the backscatter direction (172°) for the
353 incident solar irradiance over nearly cloud-free scenes. For land surfaces, such as the observations made
354 at Casper and Columbia, measurements from the POLDER satellite over China show that the backscatter
355 amount from the land surface increases with increasing wavelength (Maignan et al., 2004). For EPIC data
356 over land that are comparable to the POLDER measurements, the C/s data should be converted to
357 reflectance. When this is done, the wavelength dependence of the EPIC albedo (551, 680, and 780 nm)
358 is similar to POLDER surface reflectance even though there is no EPIC atmospheric correction and there
359 is some cloud cover.
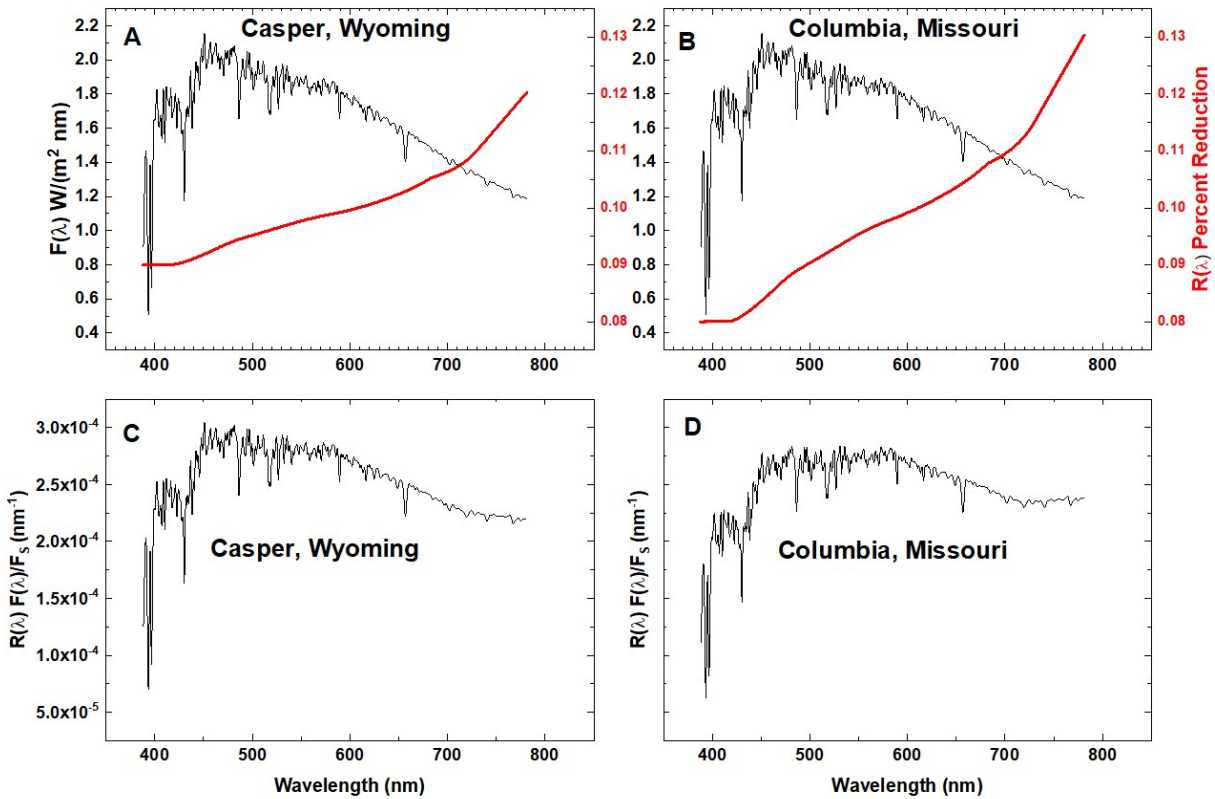
360

Fig. 10 Solar Irradiance at 1 AU F(λ) Watts/(m^2 nm) (Mayer and Kylling, 2005) and the eclipse reduction function R(λ) in percent for Casper, Wyoming (red curve in panel A) and Columbia, Missouri (red curve in panel B). Fractional reduction (nm^{-1}) in reflected solar irradiance in the direction of L-1 for Casper, Wyoming (panel C) and Columbia, Missouri (panel D)

361

362   To estimate the fractional reflected radiance reduction for the wavelength range from 388 to
363 780 nm, a polynomial interpolation R(λ) of the Avg. PD in Table 3 for the 5 weakly absorbed channels is
364 formed (Fig. 10 panels A and B red curves). R(λ) must be weighted by the solar irradiance spectrum
365 F(λ). The solar spectrum used is a combination of measured solar flux data named "atlas_plus_modtran"

366   in the libRadtran software package (Mayer and Kylling, 2005). The components, F_R and F_S, of the

367   weighted average R are defined in Eqns. 1 and 2. On 21 August 2017 the distance of the Earth from the

368   Sun was 1.011 AU, or F_S(21 Aug at 1 AU) = 664.94 W/m^2 and at 1 AU, $F_{R\text{-}Casper}$ = 66.11 W/m^2 and $F_{R\text{-}Columbia}$

369   = 64.86 W/m^2. For the wavelength range of interest (387.9 to 781.25 nm), F_S is about half of the total

370   solar irradiance of 1361 W/m^2 at the top of the atmosphere at 1 AU (Kopp and Lean, 2011), where

371

372

$$F_S = \int_{387}^{781} F(\lambda)d\lambda \qquad\qquad F_R = \int_{387}^{781} R(\lambda)F(\lambda)d\lambda \qquad (2)$$

$$<R> = \frac{\int_{387}^{781} R(\lambda)F(\lambda)d\lambda}{\int_{387}^{781} F(\lambda)d\lambda} \qquad \begin{aligned} R_{Casper} &= 0.101 \\[4pt] R_{Columbia} &= 0.098 \end{aligned} \qquad (3)$$

373   Figure 10b shows the product $R(\lambda)F(\lambda)/F_S$ (nm^{-1}). Forming R shows that during the eclipse the

374   shadow of the Moon reduces the backscattered radiance (388 to 780 nm) from the sunlit Earth in the

375   direction of L_1 by about 10 %. The combined uncertainty ±0.3 % is caused by variations in the cloud

376   cover of the reference days compared the eclipse day. The calculation of R is based on C/s

377   measurements from DSCOVR/EPIC of the sunlit Earth and the interpolation function $R(\lambda)$. The result is

378   independent of the absolute calibration of EPIC, since it is based on ratios of C/s over three days with

379   approximately the same UTC (scattering phase angles). $R(\lambda)$ includes the near backscatter direction

380   enhanced reflection function appropriate for the entire sunlit disk at a backscatter angle of about 172°.

381   The three days at nearly the same UTC can be compared directly, since EPIC has proven to be very stable

382   based on repeated in-flight calibrations over a 2-year period using OMPS and MODIS (Herman et al.,

383   2018 and Geogdzhayev and Marshak, 2018). The smooth function $R(\lambda)$ does not include absorption

384   features from water and the O_2 A- and B-bands.

385   **3.0 Summary**

386   The EPIC instrument onboard the DSCOVR spacecraft synoptically observes the entire sunlit

387   portion of the Earth from an orbit near the Earth-Sun Lagrange-1 point. On 21 August 2017, EPIC was

388   able to observe the totality shadow from the lunar eclipse of the Sun with the Earth's surface for about 3

389   hours (seven 10-channel measurements) as it crossed the United States from west to east (about 1.5

390   hours). When the region of totality was over Casper, Wyoming at 17:44:50 UTC, the reflected 443 nm

391   TOA radiance was reduced to 16 C/s (8x10^{-5} W/m^{2}sr) in the narrow region of totality compared to a non-

392   eclipse day (1.52x10^4 C/s or 0.076 W/m^{2}sr). About 30 minutes later the shadow passed over Columbia,

393   Missouri, but the presence of thin clouds in the vicinity of Columbia caused increased reflected radiance

394   of 312 C/s (1.6×10^{-3} W/m^{2}sr) during totality compared to Casper. The ratio $R_{EN}(\lambda_i)$ of reflected radiances

395   within the eclipse totality to radiances for the same geometry on adjacent non-eclipse days was

396   measured for all 10 wavelength channels. The measured R_{EN}(443 nm) was smaller for Columbia (71) than

397   for Casper (936), showing the sensitivity of increased cloud cover over Columbia. Similarly R_{EN}(388 nm,

398   Casper) = 3500 and R_{EN}(388 nm, Columbia) = 81.   While the results cannot be directly compared with

399   R_{EN}, good agreement was obtained (Kazantzidis et al., 2007) between a model study based on a 3D

400   Monte Carlo radiative transfer model (Emde and Mayer, 2007) and measured ratio at 380 nm (ratio =

401   217) of downward global surface radiation before and during totality. The measured radiance ratios

402    $R_{EN}(\lambda_i)$ can serve as a validation data set for 3D radiative transfer models of the atmosphere that include

403   cloud effects, since EPIC also measures the surrounding amount of cloud cover for the entire sunlit

404   Earth. Comparing $R_{EN}(\lambda,$ Casper) with $R_{EN}(\lambda,$ Columbia) shows that Rayleigh scattering combined with

405   low optical depth clouds can scatter light into the umbra region and reduce $R_{EN}(\lambda)$. Outside of the region

406   of totality, EPIC observed the partial eclipse shadow and the fully illuminated regions of the Earth's disk.

407   Interpolating between the percent reductions in integrated radiances (in C/s) over the sunlit globe,

408   ICs(λ_i) for the 5 measured non-absorbed wavelength channels at both locations showed that the

409   integrated reflected radiance from the Earth's sunlit disk towards L$_1$ decreased by about 10 % compared

410   to the integrated radiances measured on the days before and after the eclipse for approximately the

411   same observing geometry as occurred during the eclipse. Similar calculations comparing two non-eclipse

412   days show smaller changes in ICs (less than 0.1 %) than the eclipse-day change. The five channels that

413   are partially absorbed in the atmosphere give consistent results compared to the non-absorbed

414   channels suggesting that cloud reflectivities dominate the 317.5 to 780 nm radiances reflected back to

415   space from the sunlit Earth's disk with a contribution from Rayleigh scattering for the shorter

416   wavelengths.

417

418   **Appendix**

419   The course of the eclipse in the vicinity of Casper, Wyoming and Columbia, Missouri is shown in Fig. A1
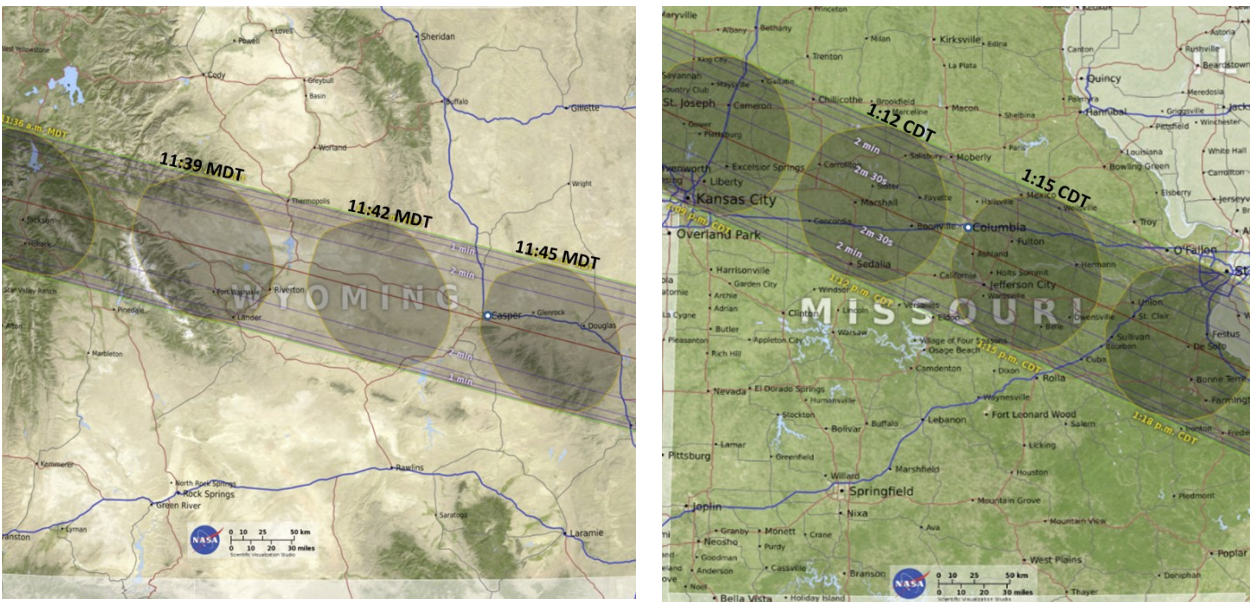
Fig. A1 The timing and shape of the Moon's shadow over Casper, Wyoming showing the relative location of Casper and Columbia (white circles) at 11:45 MDT (Mountain Daylight Time) and 1:15 CDT (Central Daylight Time). The shadow is moving at about 46 km/minute. (https://eclipse2017.nasa.gov/eclipse-maps). The NASA scale size is 50 km.

420

421

422

423 Greyscale images for the short UV wavelength channels (317.5, 325) with strong ozone absorption and
424 Rayleigh scattering, the longer wavelength UV channels (340, 388), and the strongly absorbed O_2 B- and
425 A-band channels (688, 764 nm) are shown in Figs. A2a, A2b, A2c
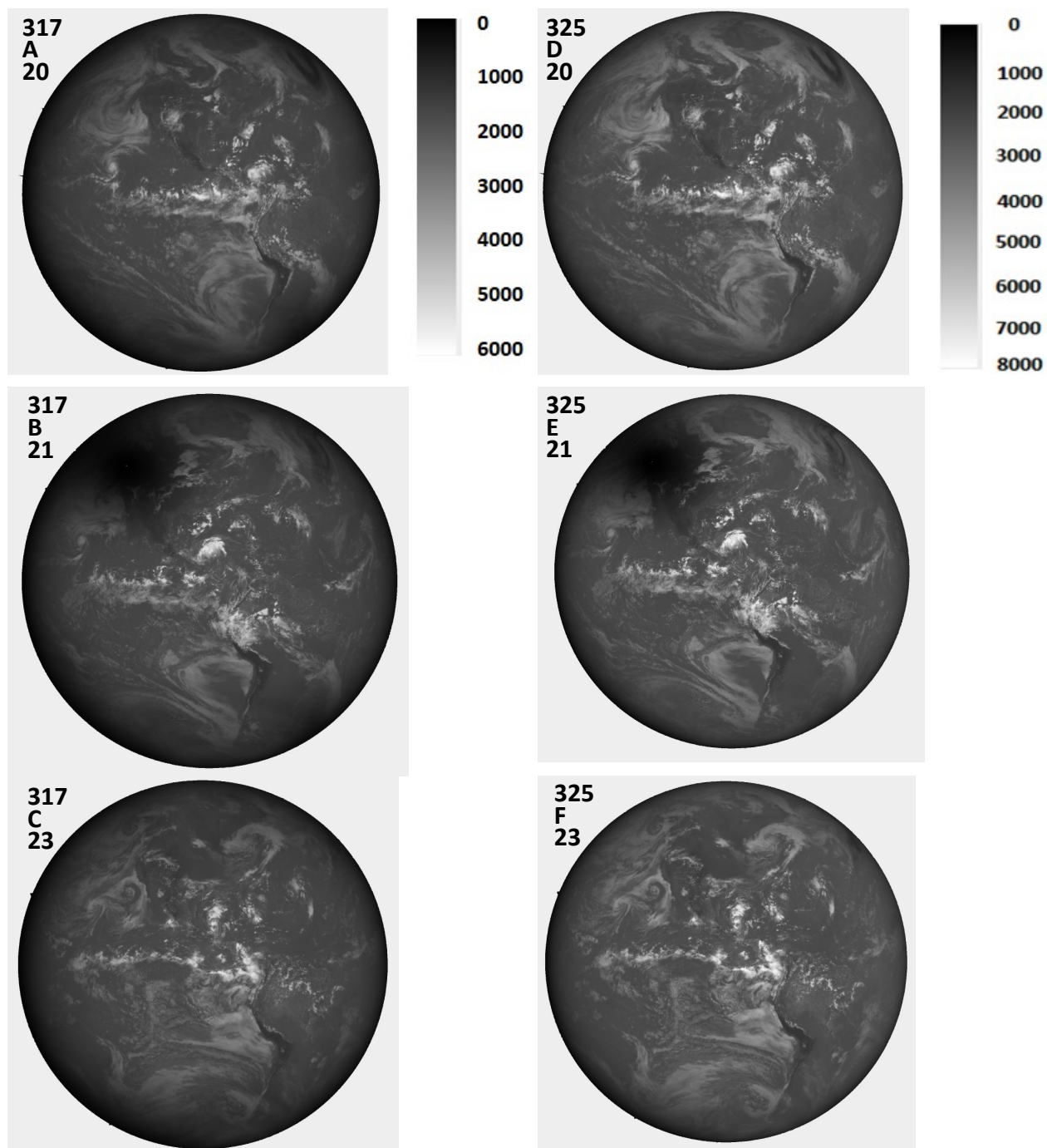
Fig. A2a Image in C/s for 317 and 340 nm for 20 Aug., 21 Aug. and 23 Aug. The scale applies to the specific wavelength. North is up.

426
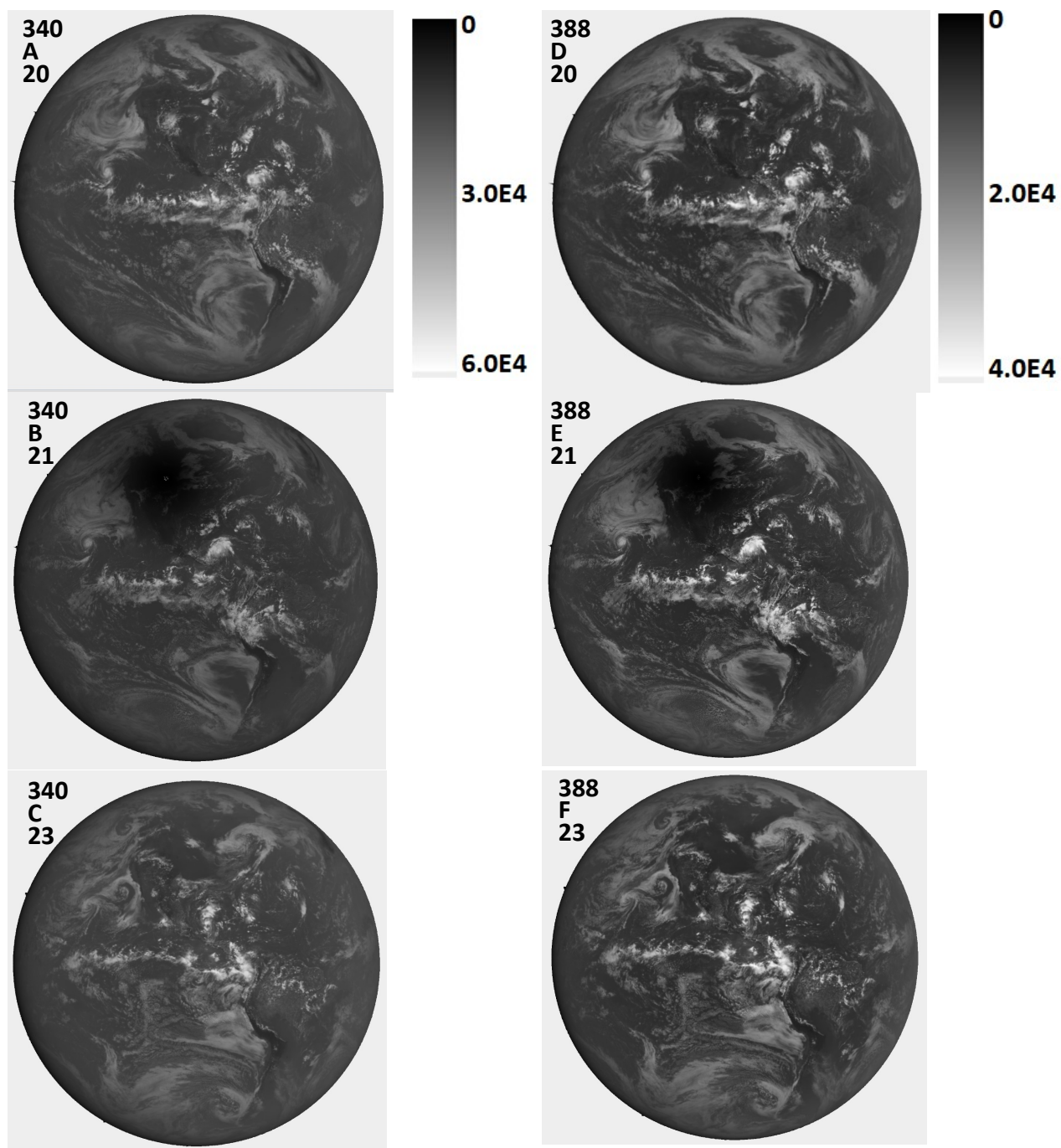
Figure A2b Image in C/s for 340 and 388 nm for 20 Aug.(A+C), 21 Aug. (B+E), and 23 Aug. (C+F). The scale applies to the specific wavelength. North is up.
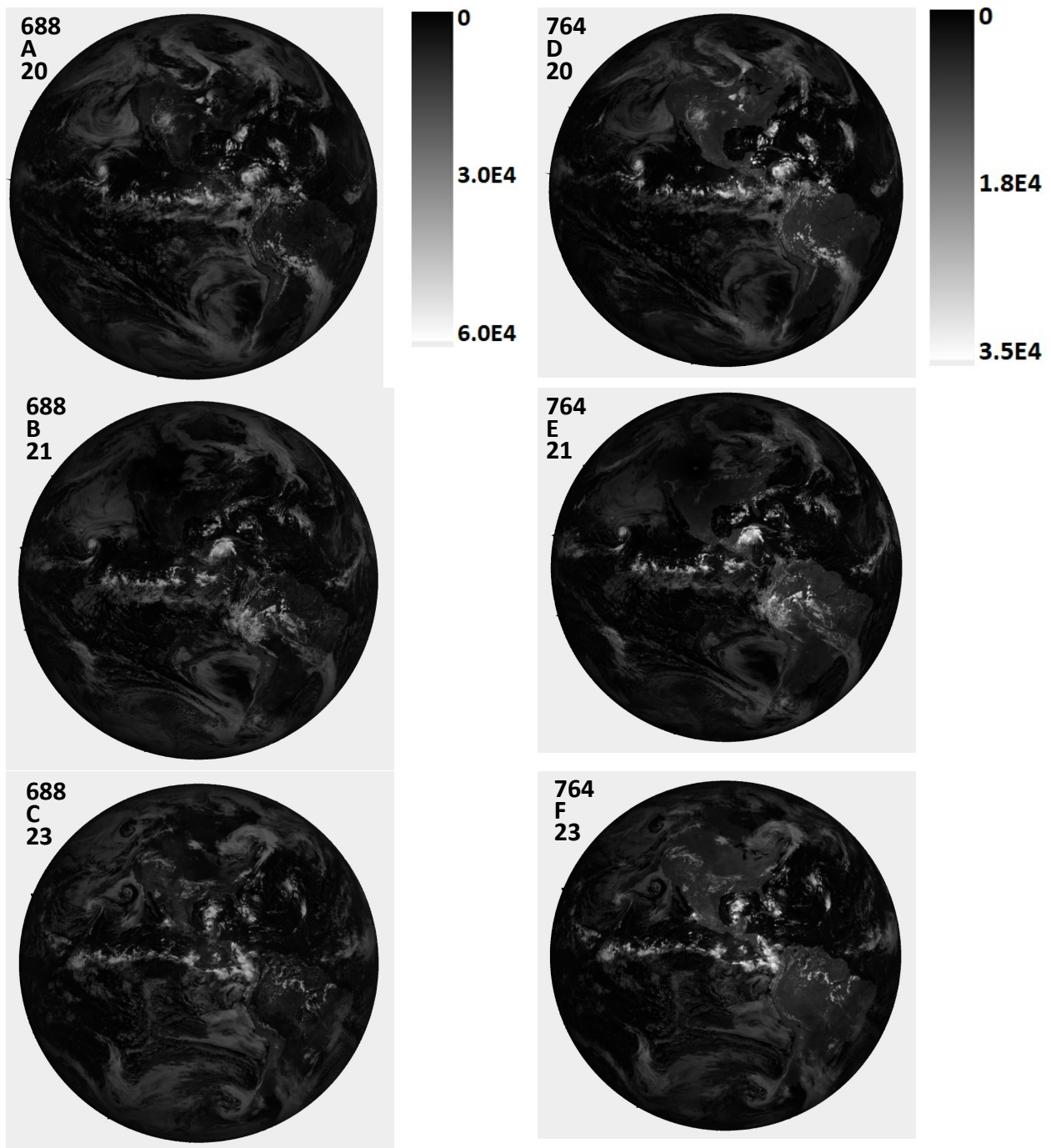
Fig. A2c Image in C/s for 688 and 764 nm for 20 Aug., 21 Aug. and 23 Aug. The scale applies to the specific wavelength. North is up.

429

430   The amount of ozone over the eclipse sites can be derived (Herman et al., 2018) to produce
431 ozone data that is stored in the NASA-Langley archive. During the eclipse, it is not possible to derive the
432 amount of ozone from either ground-based or satellite data. Ozone amounts do not change rapidly from
433 day to day except when major weather systems pass through a region, which was not the case during

434   the eclipse period, 20 August to 23 August. This is confirmed from OMI satellite data (Ozone Monitoring

435   Instrument onboard the AURA satellite). Figure A3 shows the amount of ozone over the eclipse

436   trajectory obtained on 20 August. The values obtained 316 DU near Casper, WY and 306 DU near

437   Columbia compare well with ozone amounts derived from OMI of 314 DU and 301 DU. The O_3 variability

438   during the 2.7 minutes (approximately 124 km or about 1^O of longitude) is about ±5 DU.
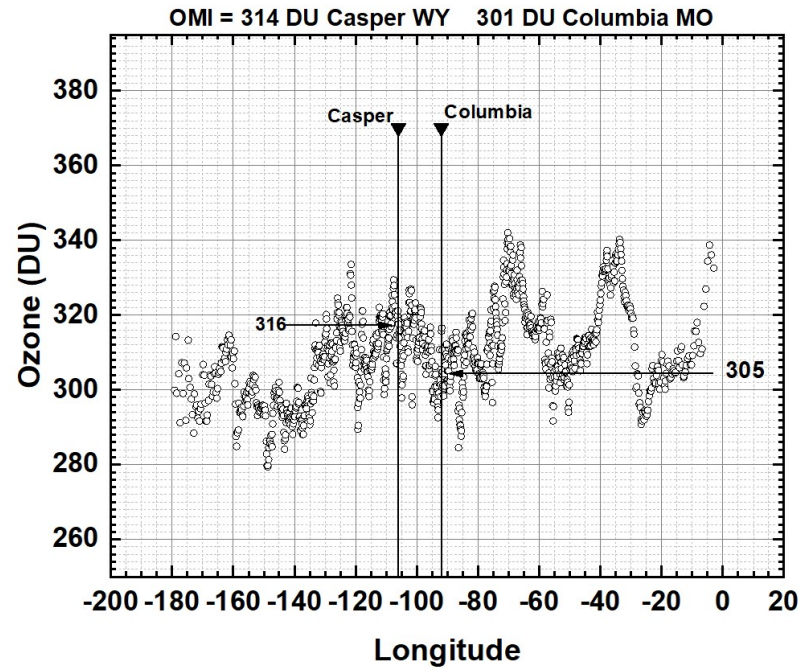
Fig. A3 EPIC measured ozone amounts from 20 August in the vicinity of Casper, WY and Columbia, MO.

439

440

441

4.0 Author Contributions

Jay Herman wrote most of the paper and performed most of the calculations

Guoyong Wen is the funded principal investigator of the project.

Alexander Marshak provided the calibration coefficients for the visible and near-IR channels

Karin Blank provided the color images in Figs. 1 to 3. She was responsible for the geolocation of the 10 filter images on a common grid.

Liang Huang provided the calibration coefficients for the UV channels

Alexander Cede provided the flatfielding, stray light correction, and dark current analysis

Nader Abuhassan helped with flatfielding and stray light correction and was responsible for the ground-based portion of this research.

Matthew Kowalewski provided the flatfielding, stray light correction, and dark current analysis

The authors declare that they have no conflict of interest.

456 **5.0 References**

457 Cleveland, William S., LOWESS: A program for smoothing scatterplots by robust locally weighted
458 regression. The American Statistician. **35** (1): 54. JSTOR 2683591. doi:10.2307/2683591, 1981.
459

460 Emde, C. and B. Mayer, Simulation of solar radiation during a total eclipse: a challenge for radiative
461 transfer,(2007) Atmos. Chem. Phys., 7, 2259–2270, 2007.

462 Geogdzhayev, I. V. and Marshak, A.: Calibration of the DSCOVR EPIC visible and NIR channels using
463 MODIS Terra and Aqua data and EPIC lunar observations, Atmos. Meas. Tech., 11, 359-368,
464 https://doi.org/10.5194/amt-11-359-2018, 2018.

465 Gerasopoulos, E., Zerefos, C. S., Tsagouri, I., Founda, D., Amiridis, V., Bais, A. F., Belehaki, A., Christou, N.,
466 Economou, G., Kanakidou, M., Karamanos, A., Petrakis, M., and Zanis, P.: The total solar eclipse of March
467 2006: overview, Atmos. Chem. Phys., 8, 5205-5220, https://doi.org/10.5194/acp-8-5205-2008, 2008.

468 Herman, J.R., Alexander Cede, Elena Spinei, George Mount, Maria Tzortziou, Nader Abuhassan, (2009)
469 NO_2 Column Amounts from Ground-based Pandora and MFDOAS Spectrometers using the Direct-Sun
470 DOAS Technique: Intercomparisons and Application to OMI Validation, J. Geophys. Res., 114, D13307,
471 doi:10.1029/2009JD011848, 2009.
472

473 Herman, J.R., R.D. Evans, A. Cede, N.K. Abuhassan, I. Petropavlovskikh, and G. McConville, (2015)
474 Comparison of Ozone Retrievals from the Pandora Spectrometer System and Dobson
475 Spectrophotometer in Boulder Colorado, Atmos. Meas. Tech., 8, 3407–3418, 2015 doi:10.5194/amt-8-
476 3407-2015
477

478 Herman, Jay, Liang Huang, Richard McPeters, Jerry Ziemke, Alexander Cede, and Karin Blank, Synoptic
479 ozone, cloud reflectivity, and erythemal irradiance from sunrise to sunset for the whole earth as viewed
480 by the DSCOVR spacecraft from the earth–sun Lagrange 1 orbit, 2017, Atmos. Meas. Tech., 10, 1–18,
481 https://doi.org/10.5194/amt-10-1-2017.

482 Ji, Q. and S.-C. Tsay (2000) On the dome effect of Eppley oyrgeometers and pyranometers, Geophys.
483 Res. Lett.m 27:971-974.

484 Kazantzidis, A., Bais, A. F., Emde, C., Kazadzis, S., and Zerefos, C. S.: Attenuation of global ultraviolet and
485 visible irradiance over Greece during the total solar eclipse of 29 March 2006, Atmos. Chem. Phys., 7,
486 5959-5969, https://doi.org/10.5194/acp-7-5959-2007, 2007.

487 Kopp, G.; Lean, J. L., (2011), A new, lower value of total solar irradiance: Evidence and climate
488 significance, *Geophysical Research Letters*. **38**.

489   Littmann, Mark; Espenak, Fred; *Wilcox*, Ken (2008). Totality: Eclipses of the Sun. Oxford University
490 Press. pp. 18–19. ISBN 0-19-953209-5.

491 Liendo, J.A. and G.H. Chacin, (2004), A study of a solar eclipse using a photocell, Revista Brasileira de
492 Ensino de Fisica, v. 26, 395 – 399.

493 Maignan, F., Breon, F. M., and Lacaze, R., (2004), Bidirectional reflectance of Earth targets: Evaluation of
494 analytical models using a large set of spaceborne measurements with emphasis on the Hot Spot,
495 Remote Sens. Environ., 90, 210–220, doi:10.1016/j.rse.2003.12.006.

496 Marshak, Alexander, Jay R. Herman, Adam Szabo, Karin B. Blank, Alexander Cede, Simon A. Carn, Igor V.
497 Geogdzhaev, Dong Huang, Liang-Kang Huang, Yuri Knyazikhin, Matthew G. Kowalewski, Nickolay A.
498 Krotkov, Alexei I. Lyapustin, Richard D. McPeters, Omar O. Torres and Yuekui Yang**, Earth Observations
499 from DSCOVR/EPIC Instrument, BAMS, accepted, 2018
500
501 Mayer, B. and Kylling, (2005) A.: Technical Note: The libRadtran software package for radiative transfer
502 calculations: Description and examples of use, Atmos. Chem. Phys., 5, 1855–1877, http://www.atmos-
503 chem-phys.net/5/1855/2005/.
504
505 Meeus, J. (2003). "The maximum possible duration of a total solar eclipse". *Journal of the British*
506 *Astronomical Association*. **113** (6): 343–48.

507 Psiloglou, B.E. and H. D. Kambezidis, Performance of the meteorological radiation model during the solar
508 eclipse of 29 March 2006, Atmos. Chem. Phys., 7, 6047–6059, 2007.

509 Wen, G., A. Marshak, and R.F. Cahalan, (2008) Importance of molecular Rayleigh scattering in the
510 enhancement of clear sky radiance in the vicinity of boundary layer cumulus clouds. J. Geophys. Res.,
511 113: [10.1029/2008JD010592].

512

513
514 Acknowledgement

519

520   **Tables**

521

Table 1 *Eclipse Measurement Timing and Location Details for 5 Wavelengths*

Eclipse Maximum and EPIC Image Times. Total Measurement Duration 2.7 minutes

Wavelength (nm)	Date and Time	Location Name	Longitude
	2017-08-21 17:35:40	Eclipse West Edge of WY state	$-111^{o}02'$
551	2017-08-21 17:42:36	West of Casper	$-106^{o}22'$
680	2017-08-21 17:43:30	West of Casper	$-106^{o}21'$
Casper Wyoming	2017-08-21 17:43:51	Casper WY	$-106^{o}19'$
780	2017-08-21 17:44:24	Near Glenrock WY	$-105^{o}52'$
443	2017-08-21 17:44:50	West of Douglas WY	$-105^{o}14'$
388	2017-08-21 17:45:18	West of Douglas WY	$-105^{o}17'$
	2017-08-21 17:48:04	Eclipse East Edge of WY state	$-104^{o}03'$

522

523

524

Table 2 *Radiance Ratio $R_{EN}(\lambda_i)$ during eclipse totality 17:45 UTC compared to 20 Aug*

Wavelength λ_i (nm)	Max. $R_{EN}(\lambda_i)$ C/s
317.5	118
325	68.2
340	144
388	86
443	122
551	119.5
680	80
688	38
764	108
780	112.5

525

526

527

528

529

530

531

532

Table 3A Eclipse change in reflected light at Casper, WY from 20, 21, 23 August 2017 Units are ICs x 10^{-7}

λ_i (nm)	20 August 2017 16:58:31 GMT	21 August 2017 17:44:50	23 August 2017 17:54:36	Avg. PD
317.5	280.5	258.8	282.0	9±0.3
325	460.6	425.5	464.2	9±0.4
340	3183	2946	3213	9±0.5
388	2034	1878	2044	9±0.3
443	5808	5344	5813.2	9±0.05
551	5619	5078	5573	10±0.5
680	3790	3433	3773	10±0.3
688	1129	1010	1110	11±0.9
764	671.9	585.9	651.9	13±1.7
780	2794	2491	2799	12±0.1

533

Table 3B Eclipse change in reflected light at Columbia, MO from 20, 21, 23 August 2017 Units are ICs x 10^{-7}

λ_i (nm)	20 August 2017 18:03:359 GMT	21 August 2017 18:14:50	23 August 2017 17:54:36	Avg. PD
317.5	281.3	258.3	282.0	9±0.1
325	461.6	425.9	464.2	9±0.3
340	3193	2956	3213	8±0.3
388	2034	1884	2044	8±0.3
443	5813.7	5372.3	5813.2	8±0.01
551	5586	5091	5573	10±0.1
680	3790	3453	3773	10±0.2
688	1121	1011	1110	10±0.5
764	661.2	576.0	651.9	14±0.8
780	2794	2475	2799	13±0.1

534

535

536

537

36

571   Fig. 9 Average reflected light in C/s for eclipse (21 Aug. red) and non-eclipse (20 Aug. and 23 Aug. (black

572   and grey) days from Table 3 and Eqn. 1 for Casper and Columbia. The locations of the maxima are from

573   curve fitting to the discrete wavelength measurements.

574   Fig. 10 Solar Irradiance at 1 AU F(λ) Watts/(m^2 nm) (Mayer and Kylling, 2005) and the eclipse reduction

575   function R(λ) in percent for Casper, Wyoming (red curve in panel A) and Columbia, Missouri (red curve

576   in panel B). Fractional reduction (nm^{-1}) in reflected solar irradiance in the direction of L-1 for Casper,

577   Wyoming (panel C) and Columbia, Missouri (panel D)

578   Fig. A1 The timing and shape of the Moon's shadow over Casper, Wyoming showing the relative location

579   of Casper and Columbia (white circles) at 11:45 MDT (Mountain Daylight Time) and 1:15 CDT (Central

580   Daylight Time). The shadow is moving at about 46 km/minute. (https://eclipse2017.nasa.gov/eclipse-

581   maps). The NASA scale size is 50 km.

582   Fig. A2a Image in C/s for 317 and 340 nm for 20 Aug., 21 Aug. and 23 Aug. The scale applies to the

583   specific wavelength. North is up.

584   Fig. A2b Image in C/s for 340 and 388 nm for 20 Aug.(A+C), 21 Aug. (B+E), and 23 Aug. (C+F). The scale

585   applies to the specific wavelength. North is up.

586   Fig. A2c A2c Image in C/s for 688 and 764 nm for 20 Aug., 21 Aug. and 23 Aug. The scale applies to the

587   specific wavelength. North is up.

588   Fig. A3 EPIC measured ozone amounts from 20 August in the vicinity of Casper, WY and Columbia, MO.

589
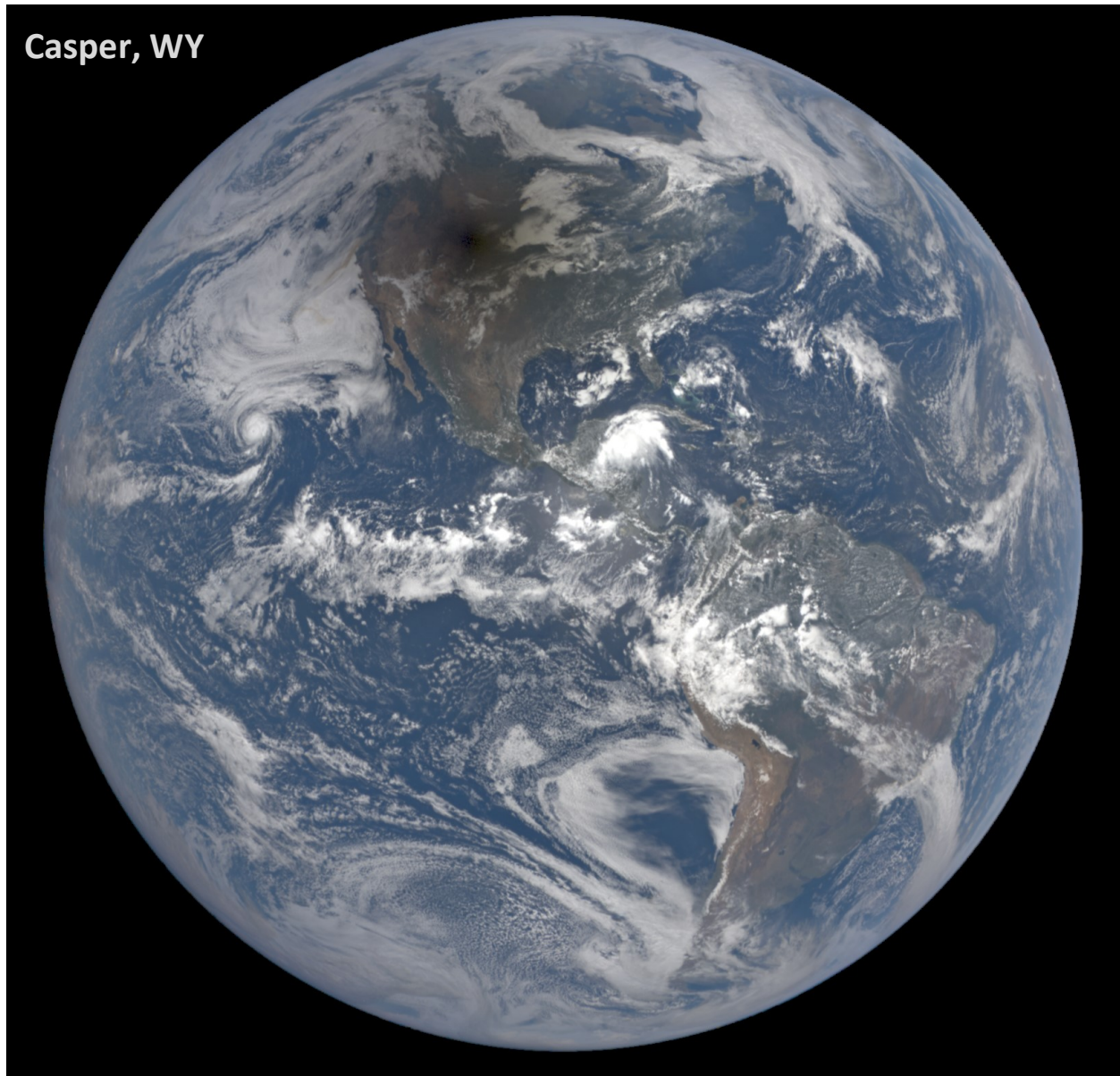
Casper, WY

Fig. 1 Synoptic view of the sunlit Earth perturbed by the 21 August 2017 total eclipse centered over Casper, Wyoming at 17:44:50 UTC. The black region is the eclipse umbra centered over Casper, WY. The color image has been adjusted from the images on https://epic.gsfc.nasa.gov/ by increasing the gamma correction to bring out the region of totality and surrounding clouds.

590

591

592   **F01**

593
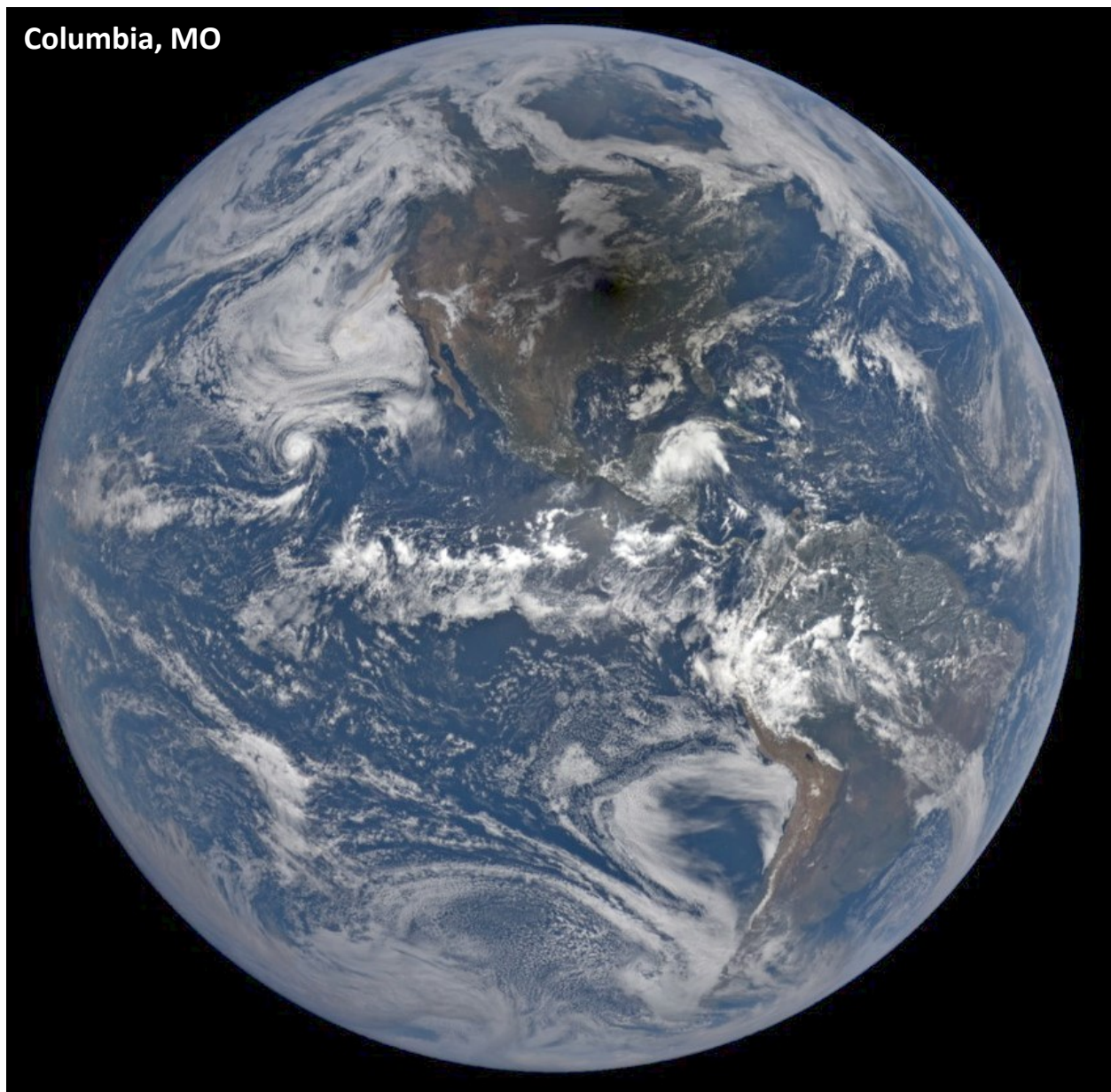
Columbia, MO

Fig. 2 Synoptic view of the total eclipse centered over Columbia, Missouri at 18:14:50 UTC. The black region is the eclipse umbra centered over Casper, WY. The color image has been adjusted from the images on https://epic.gsfc.nasa.gov/ by increasing the gamma correction to bring out the region of totality and surrounding clouds.

594

595

596 **F02**

597
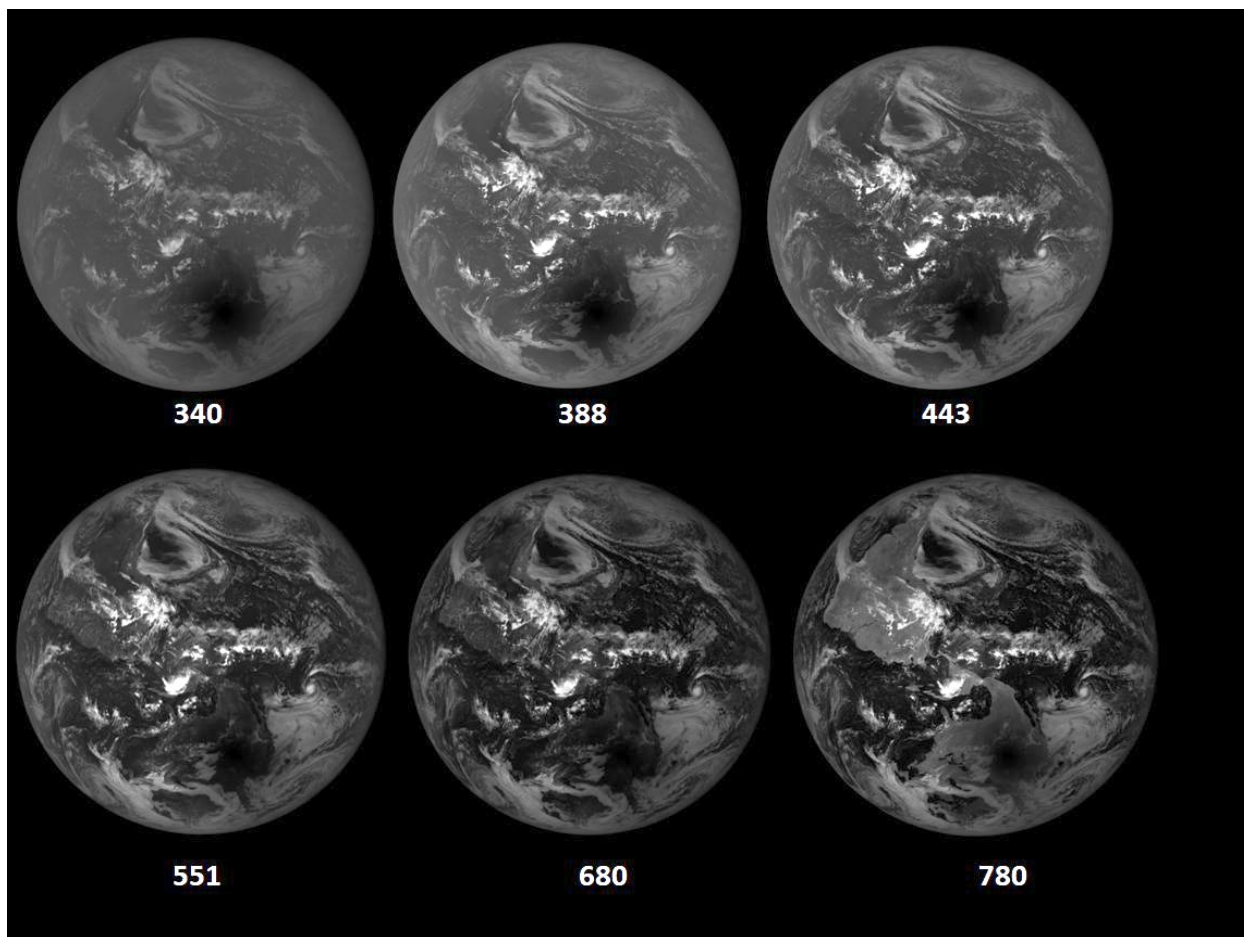
Fig. 3 Greyscale images for 6 of the DSCOVR/EPIC channels for the eclipse over Casper Wyoming showing the blurring caused by Rayleigh scattering and the dark land and ocean surfaces at 340 nm to the almost clear atmosphere and bright continental surfaces at 780 nm. The images were obtained over a period of 2.7 minutes. North is facing down.

598

599

600   **F03**
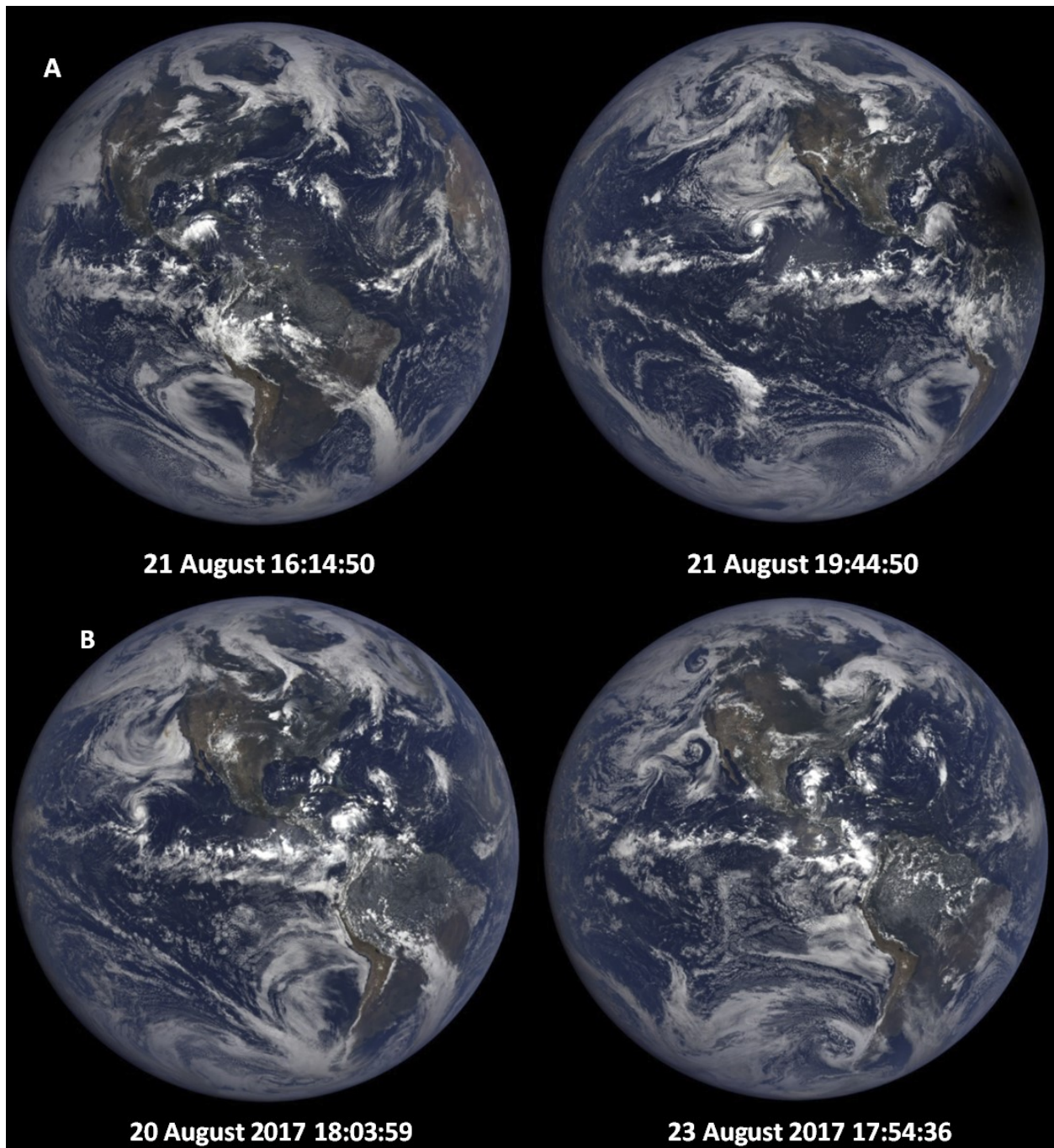
Fig. 4 Panel A: Synoptic natural color images on 21 August at 16:14 and 19:44 before and after the eclipse over the US, and Panel B: the days before and after the eclipse selected to be as close as possible to the phase angle (UTC 17:44:50) as the time of totality over Casper, Wyoming. North is facing up.

601

602 **F04**

603
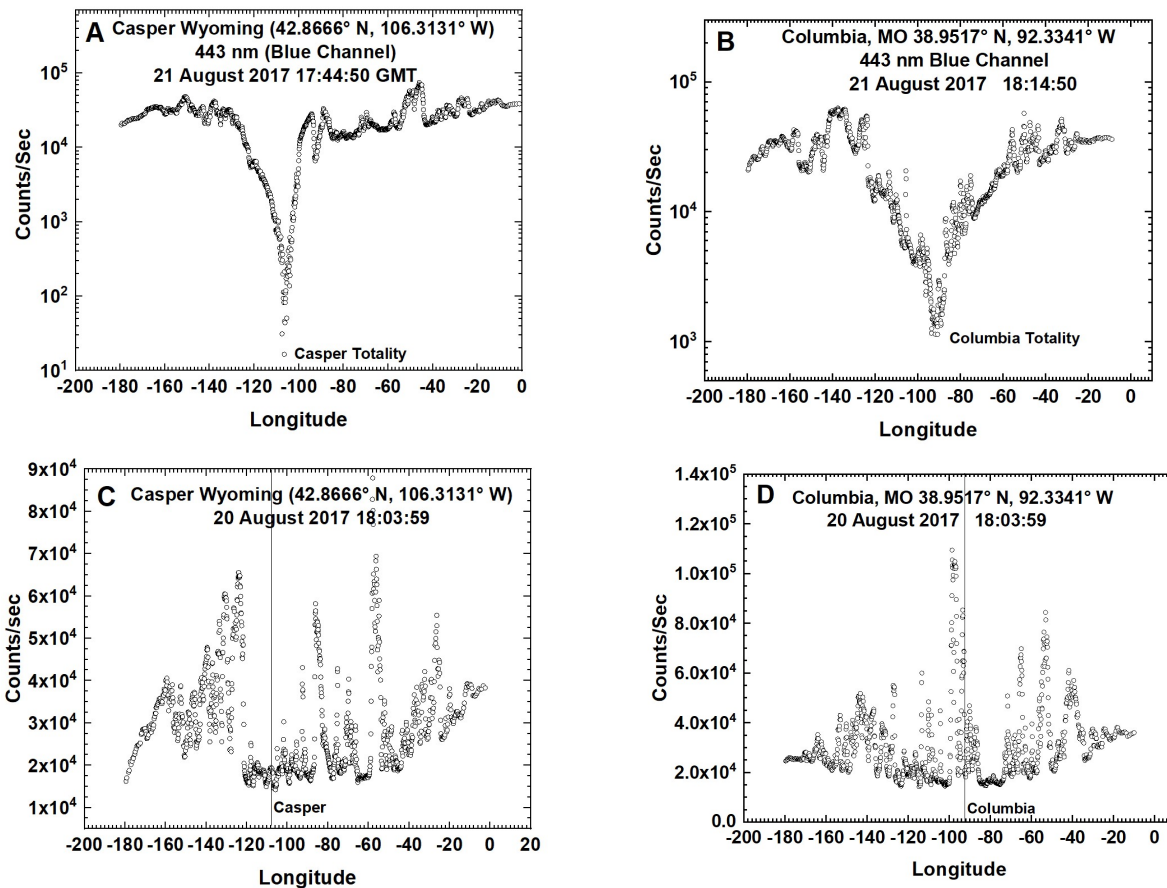
Fig. 5 Top: The effect of an eclipse (21 Aug) on the measured C/s reflected back to space as a function of longitude (degrees) for two locations, Casper Wyoming (left) and Columbia Missouri (right). Middle: Measured C/s reflected back to space on 20 Aug.

604

605

F05

607

608
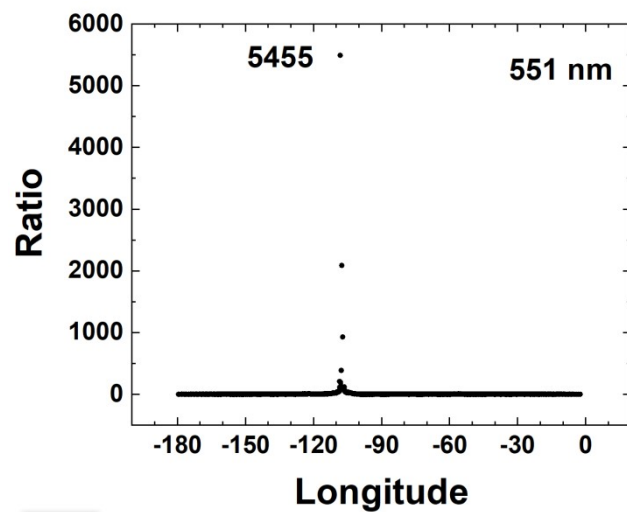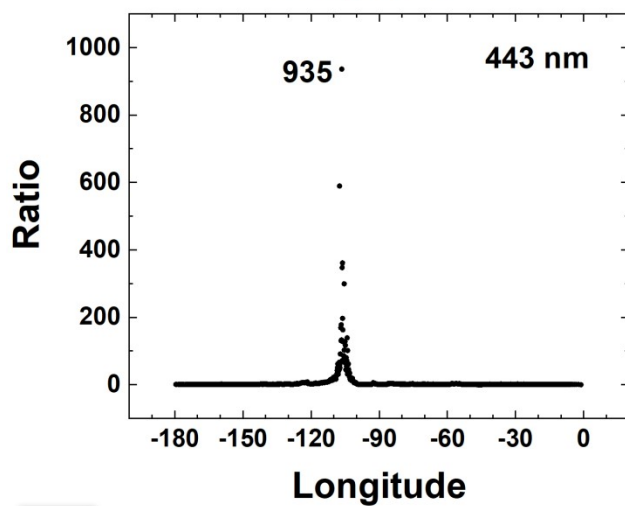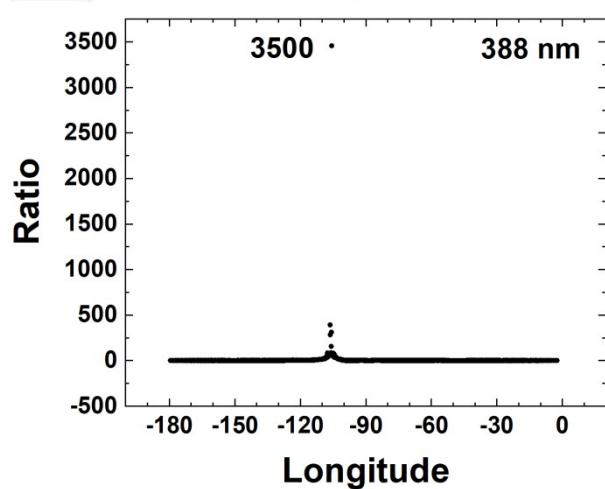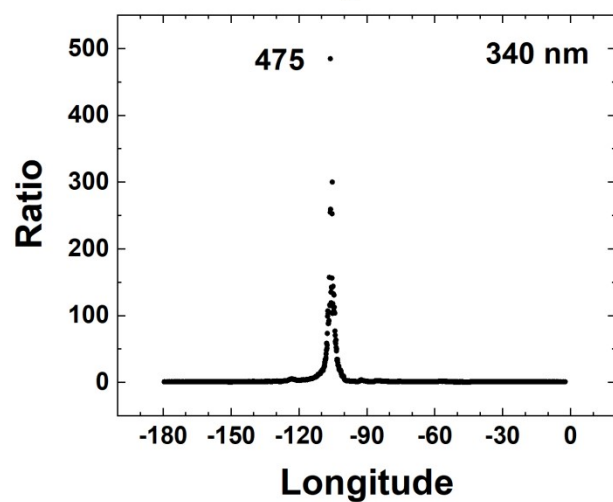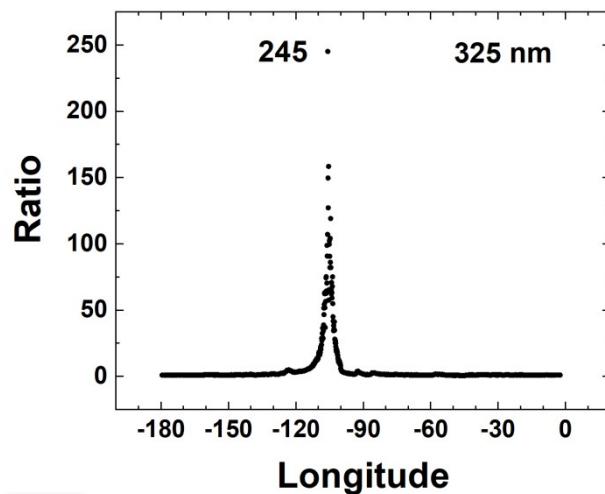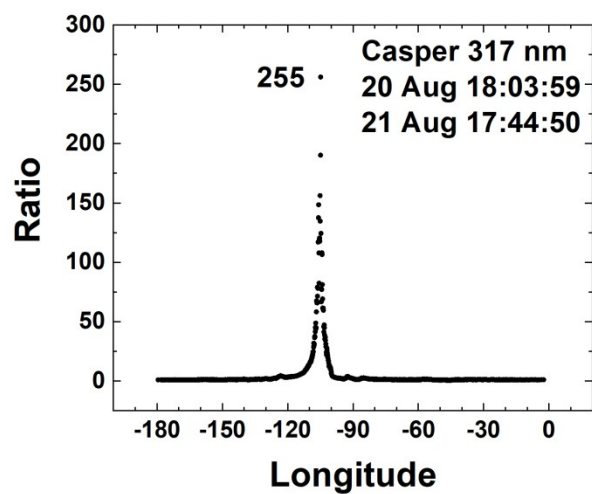
F06a

Fig. 6a. The ratio $R_{EN}(\lambda_i) = I(Aug20)/I(Aug21)$ at the time of the Eclipse in Casper Wyoming for wavelengths 317.5 to 780 nm. The channels 317.5 to 240 nm are affected by ozone absorption and the channels 688 and 764 nm are within the O_2 B and A absorption bands.

610

611
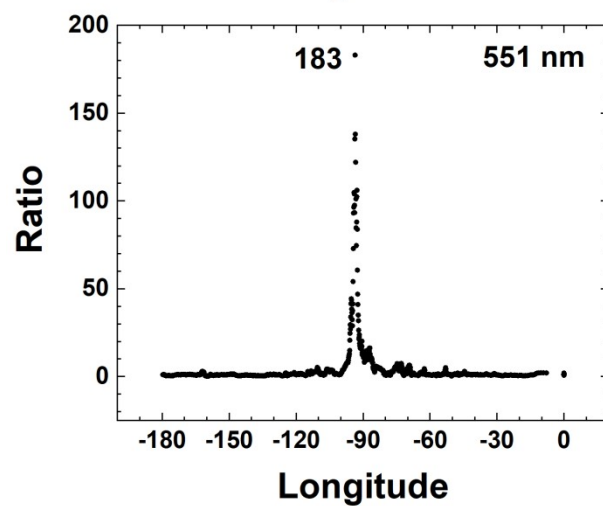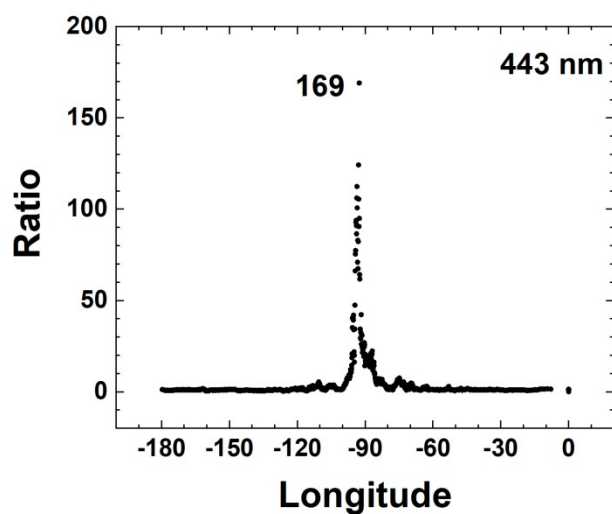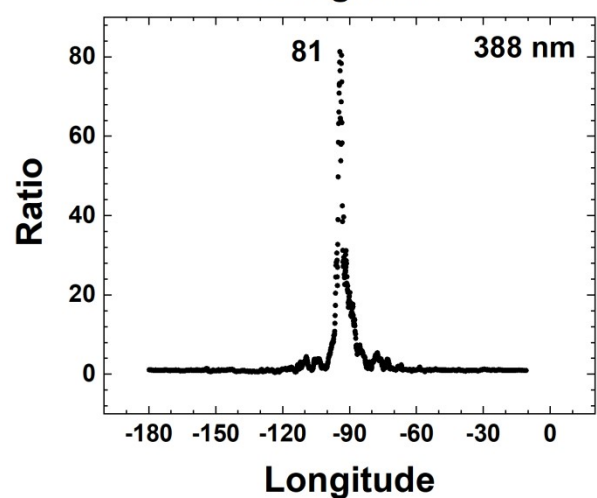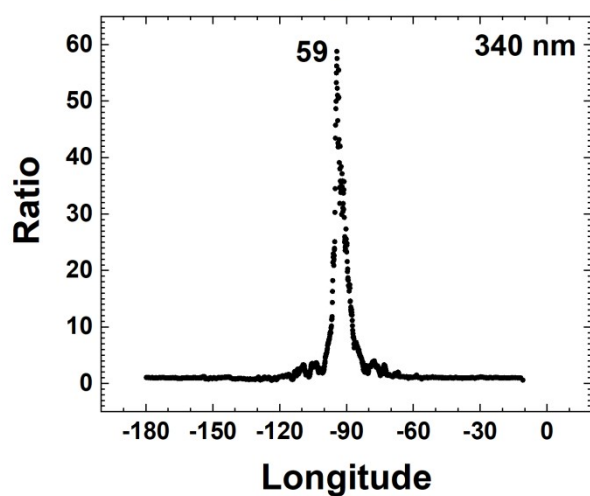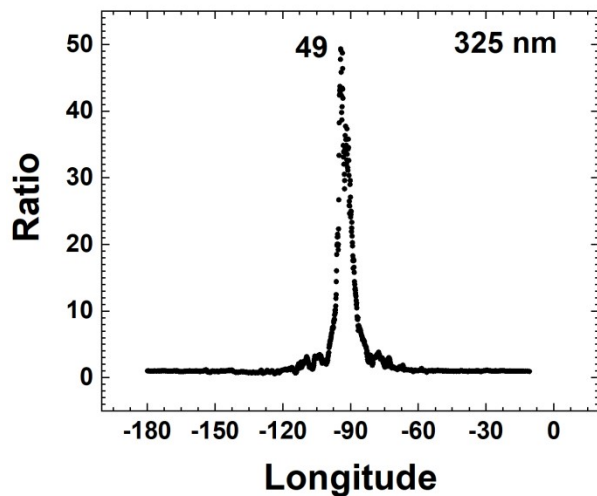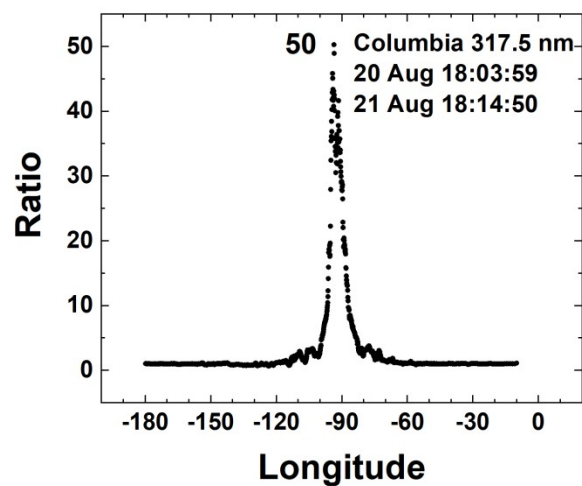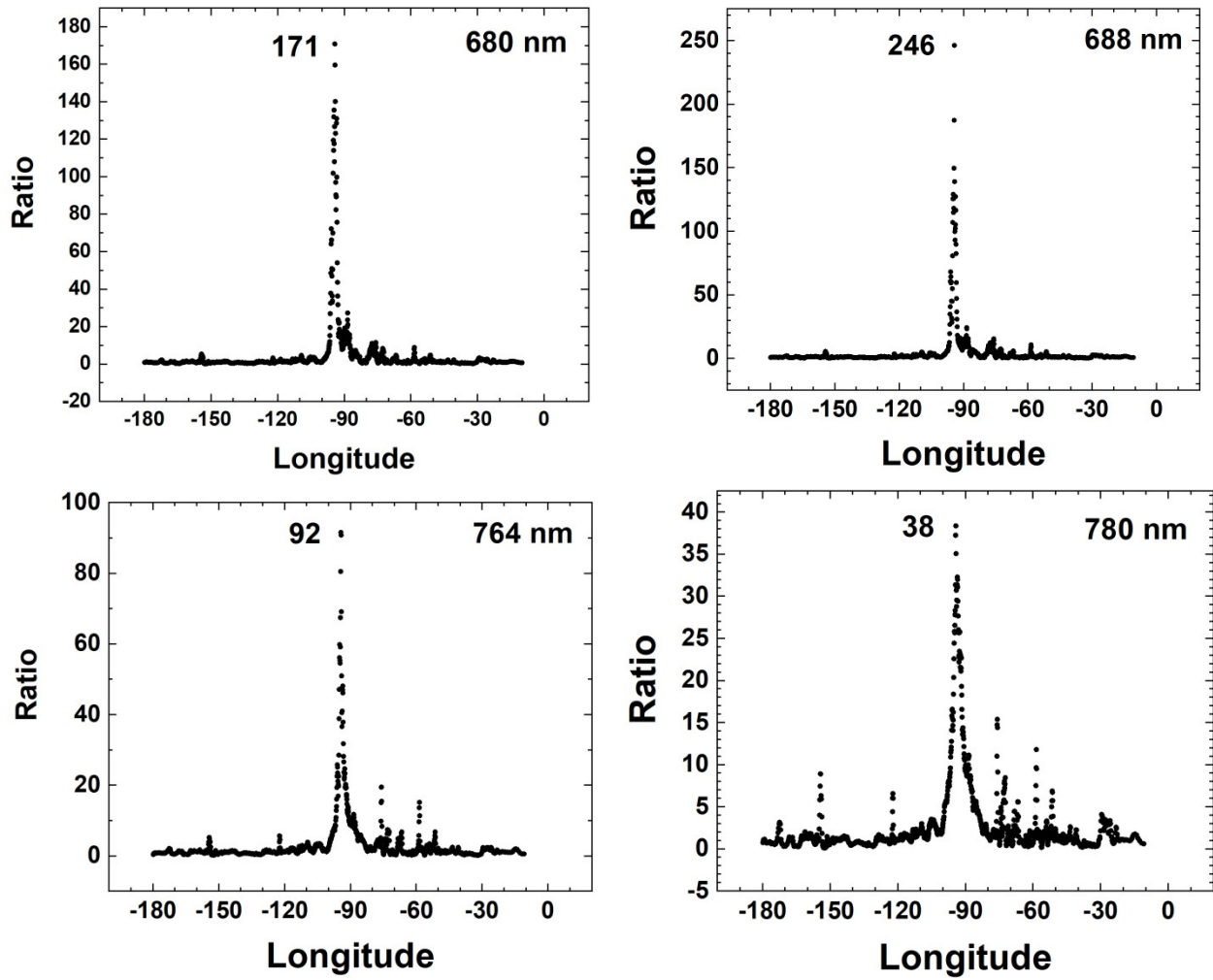
F06a Continued

44

613

F06b

45

Fig. 6b. The ratio $R_{EN}(\lambda_i) = I(Aug20)/I(Aug21)$ at the time of the Eclipse in Columbia, Missouri for wavelengths 317.5 to 780 nm. The channels 317.5 to 340 nm are affected by ozone absorption and the channels 688 and 764 nm are within the O_2 B and A absorption bands.

615

616

617

618   **F06b   Continued**

619

620
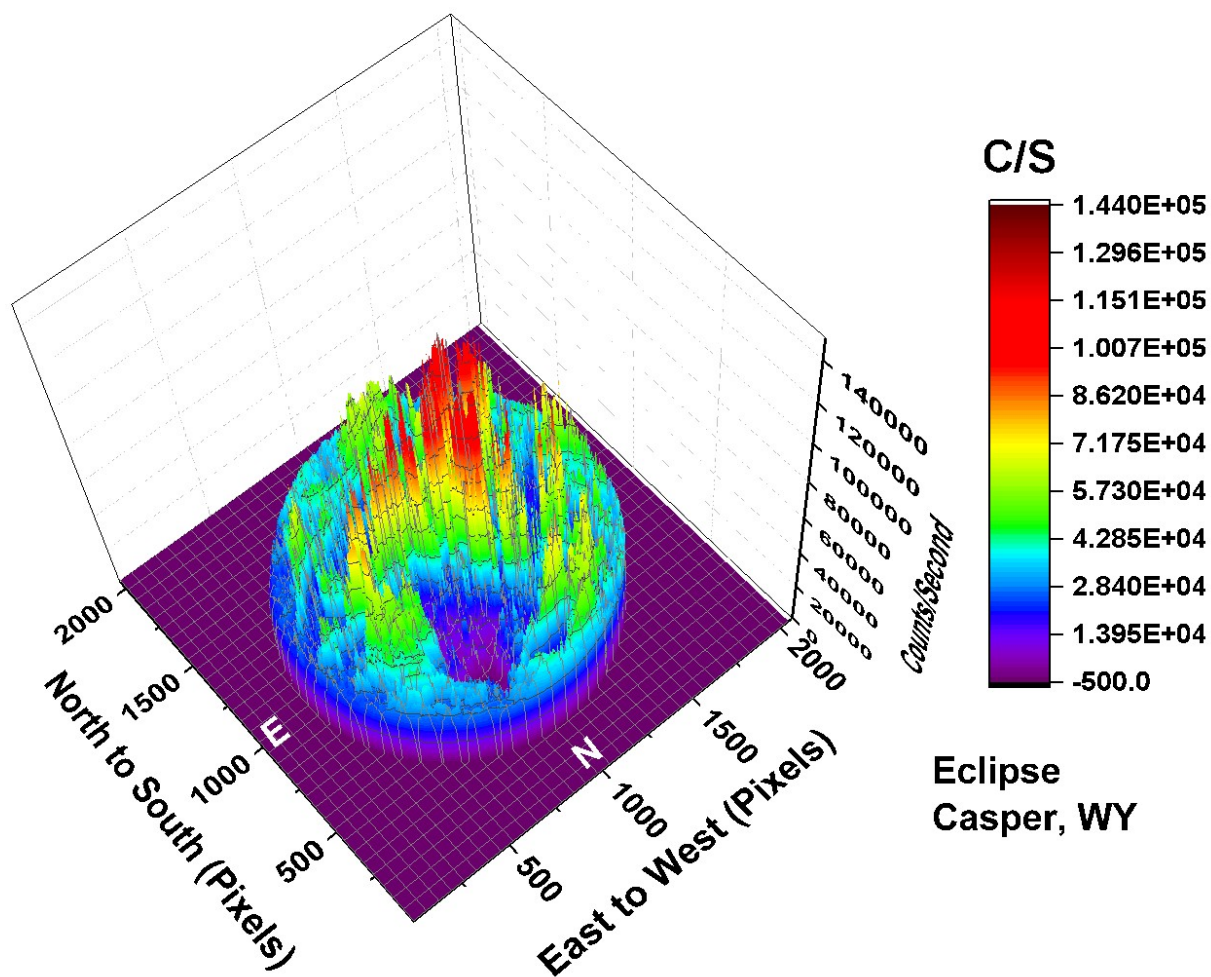
Fig. 7 The C/s observed by EPIC for the 443 nm channel corresponding to the color image shown in Fig. 1. In the data file, the word infinity has been replaced by the number zero. In this image there are approximately 2.59×10^6 illuminated pixels out of $2048^2 = 4.194304 \times 10^6$ pixels (61.8 %).

621

622

623 **F07**

624
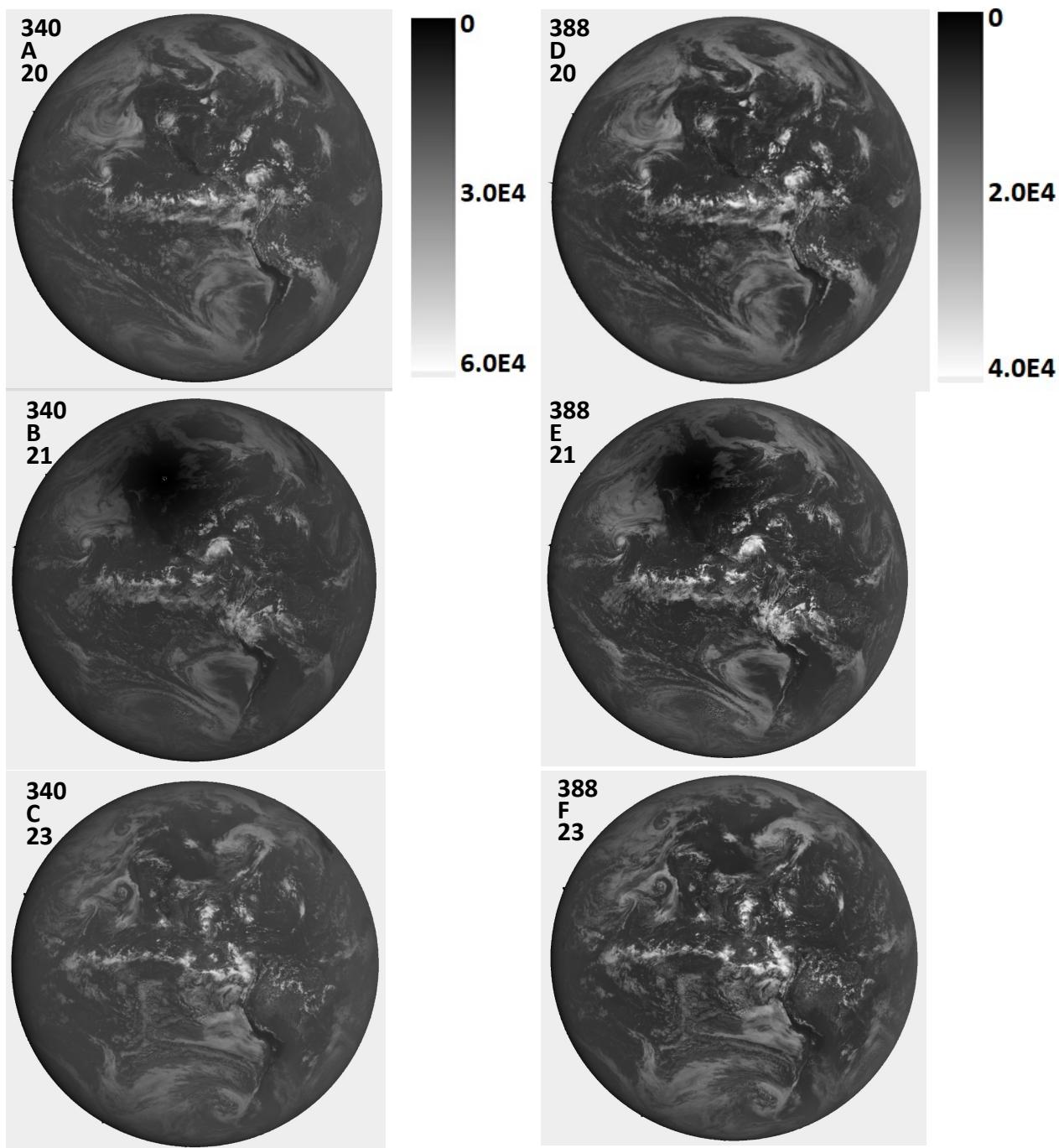
Figure 8a Image in C/s for 340 and 388 nm for 20 Aug.(A+C), 21 Aug. (B+E), and 23 Aug. (C+F). The scale applies to the specific wavelength. North is up.

625

F08a
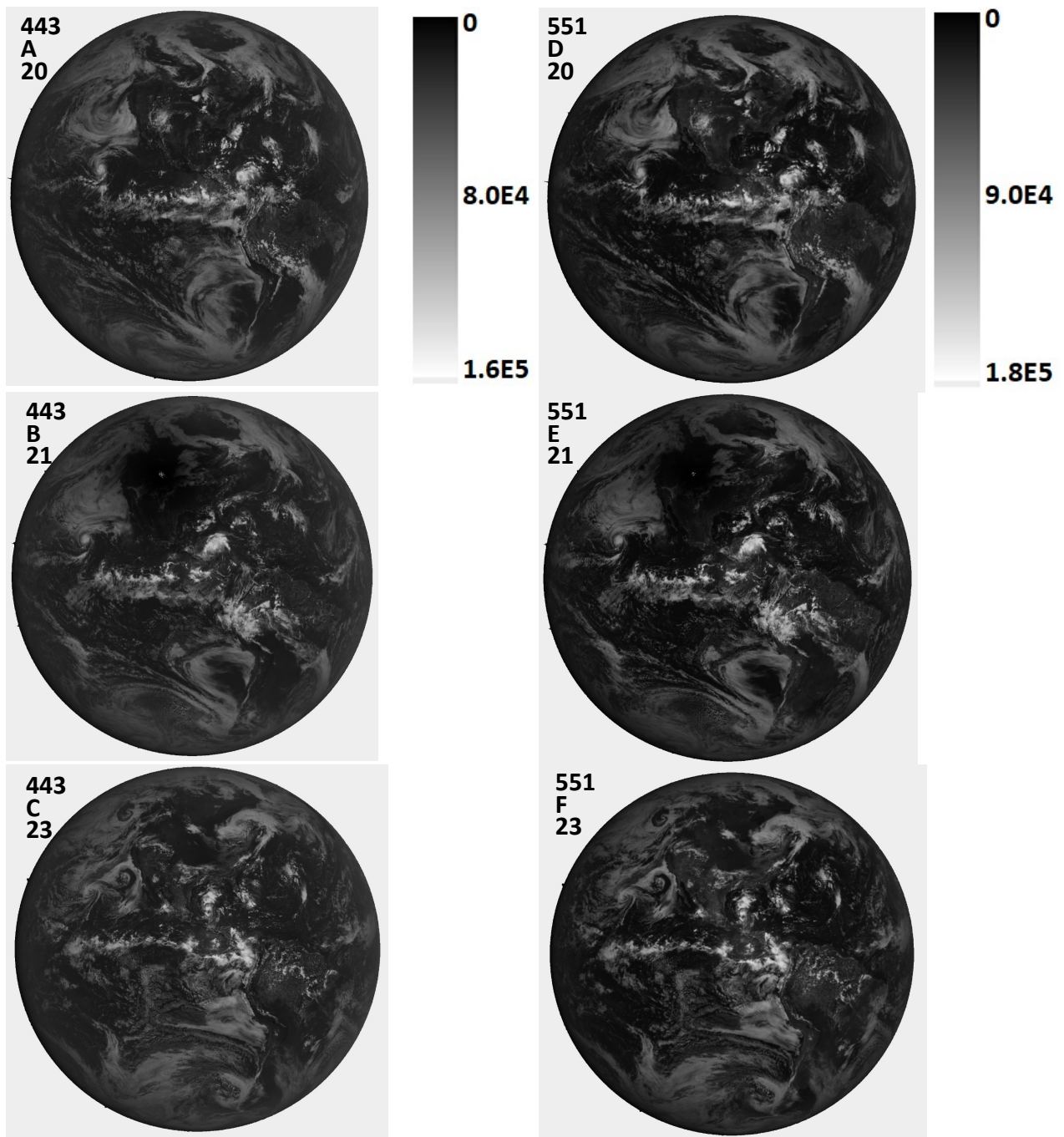
Figure 8b Image in C/s for 443 and 551 nm for 20 Aug.(A+C), 21 Aug. (B+E), and 23 Aug. (C+F). The scale applies to the specific wavelength. North is up.
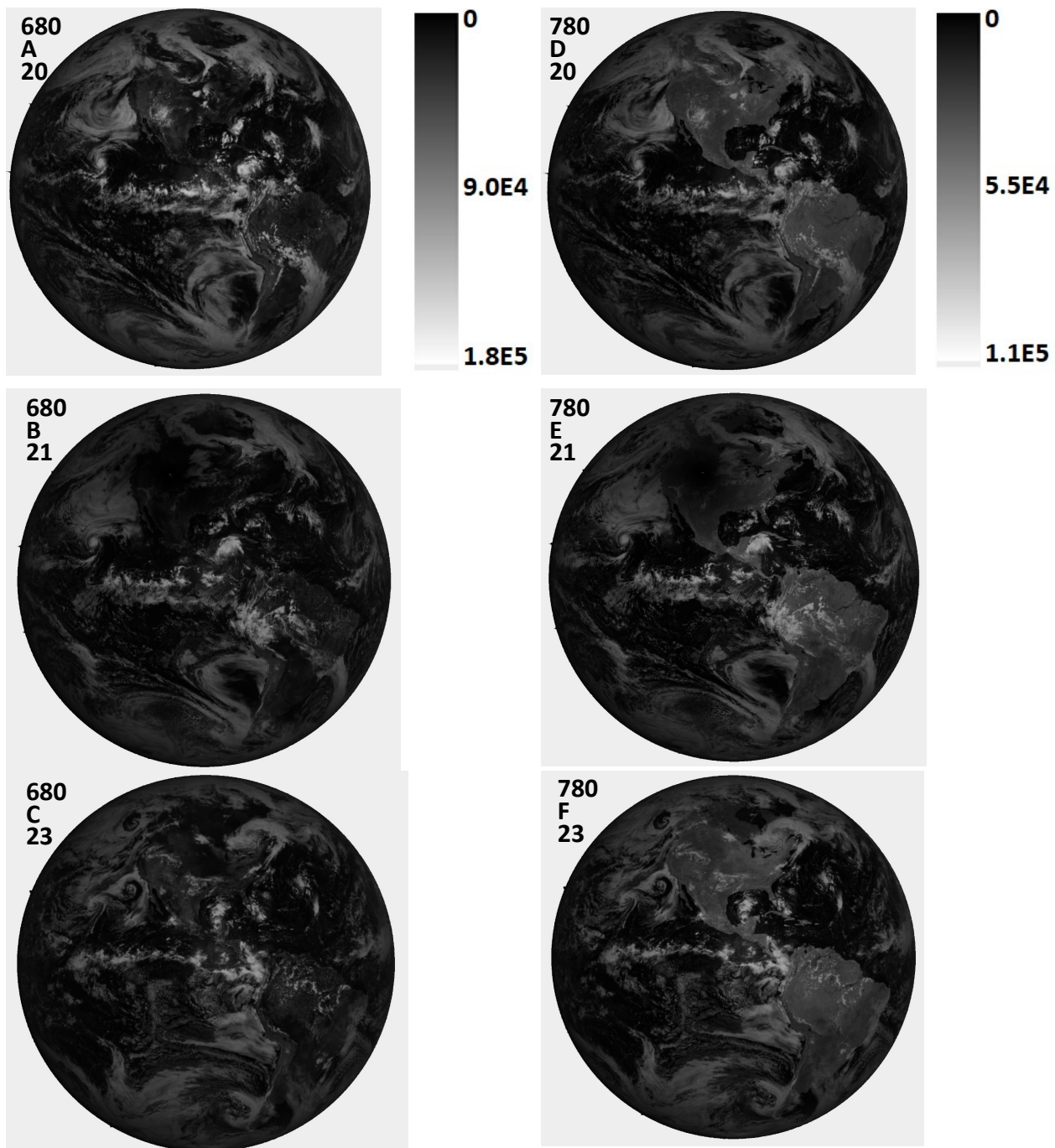
626

627

F08b

Figure 8c Image in C/s for 680 and 780 nm for 20 Aug.(A+C), 21 Aug. (B+E), and 23 Aug. (C+F). The scale applies to the specific wavelength. North is up.
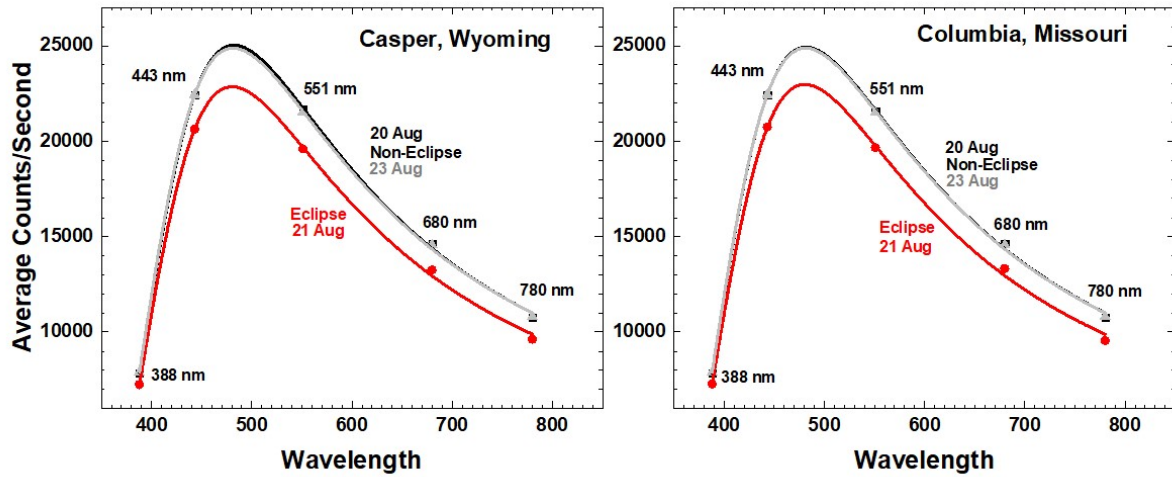
629

630

F08c

632

Fig. 9 Average reflected light in C/s for eclipse (21 Aug. red) and non-eclipse (20 Aug. and 23 Aug. (black and grey) days from Table 3 and Eqn. 1 for Casper and Columbia. The locations of the maxima are from curve fitting to the discrete wavelength measurements.
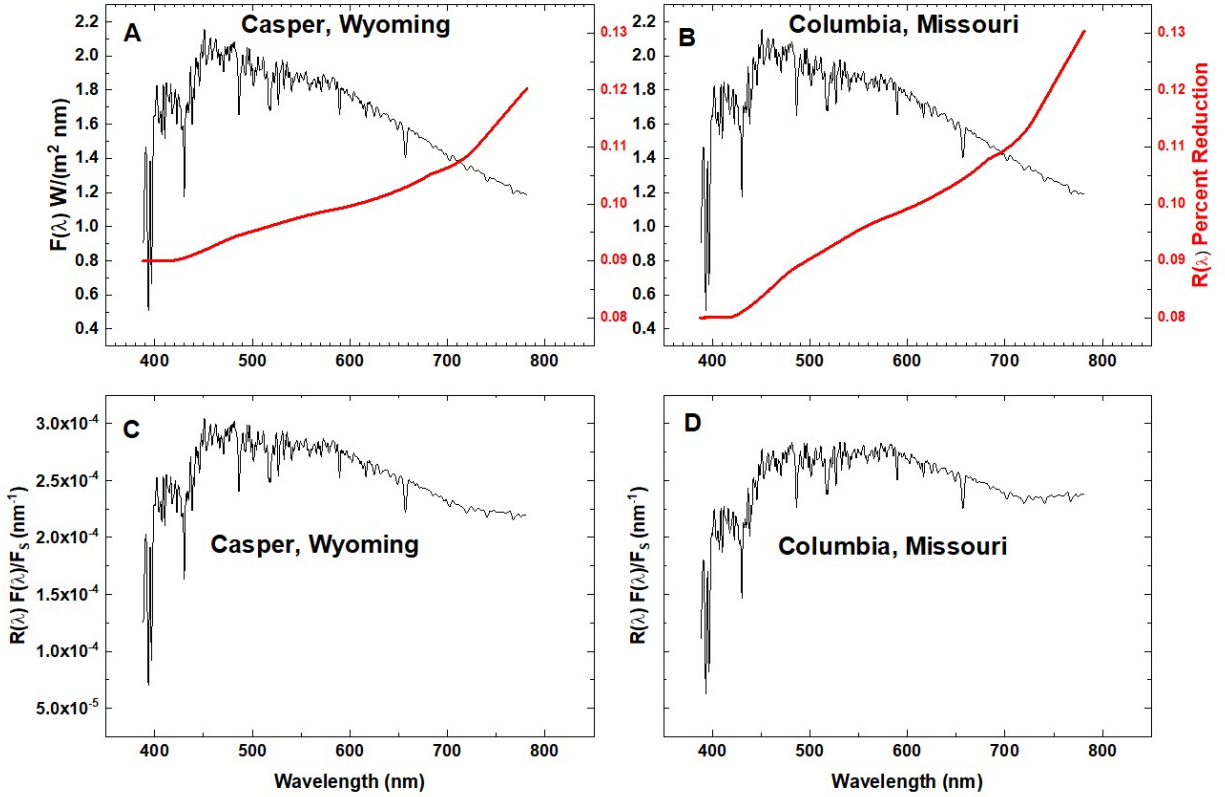
633

634

635   **F09**

Fig. 10 Solar Irradiance at 1 AU $F(\lambda)$ Watts/(m^2 nm) (Mayer and Kylling, 2005) and the eclipse reduction function $R(\lambda)$ in percent for Casper, Wyoming (red curve in panel A) and Columbia, Missouri (red curve in panel B). Fractional reduction (nm^{-1}) in reflected solar irradiance in the direction of L-1 for Casper, Wyoming (panel C) and Columbia, Missouri (panel D)

636

637

638

F10

640

641

642

Fig. A1 The timing and shape of the Moon's shadow over Casper, Wyoming showing the relative location of Casper and Columbia (white circles) at 11:45 MDT (Mountain Daylight Time) and 1:15 CDT (Central Daylight Time). The shadow is moving at about 46 km/minute. (https://eclipse2017.nasa.gov/eclipse-maps). The NASA scale size is 50 km.

643

644

645
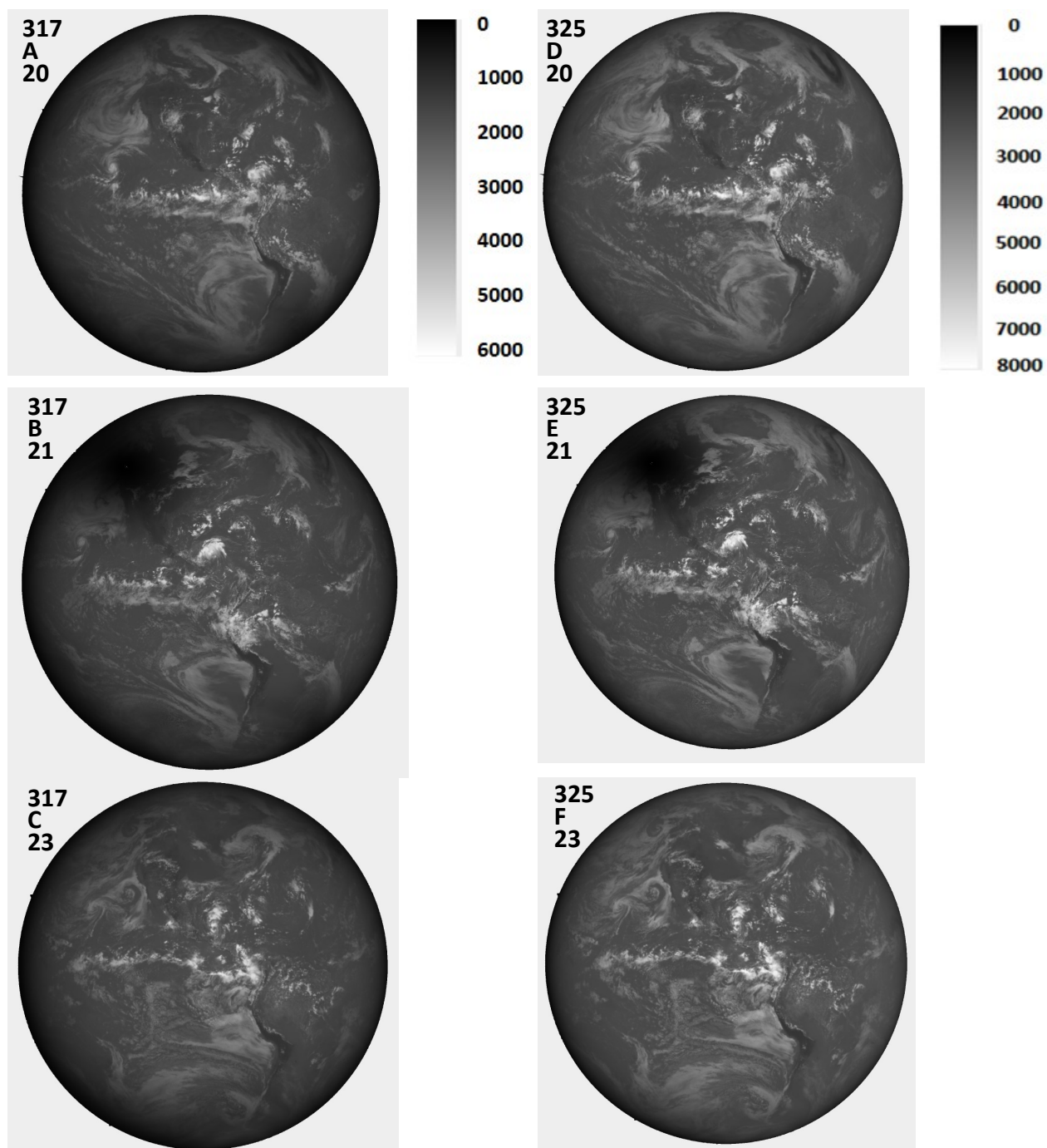
Fig. A2a Image in C/s for 317 and 340 nm for 20 Aug., 21 Aug. and 23 Aug. The scale applies to the specific wavelength. North is up.
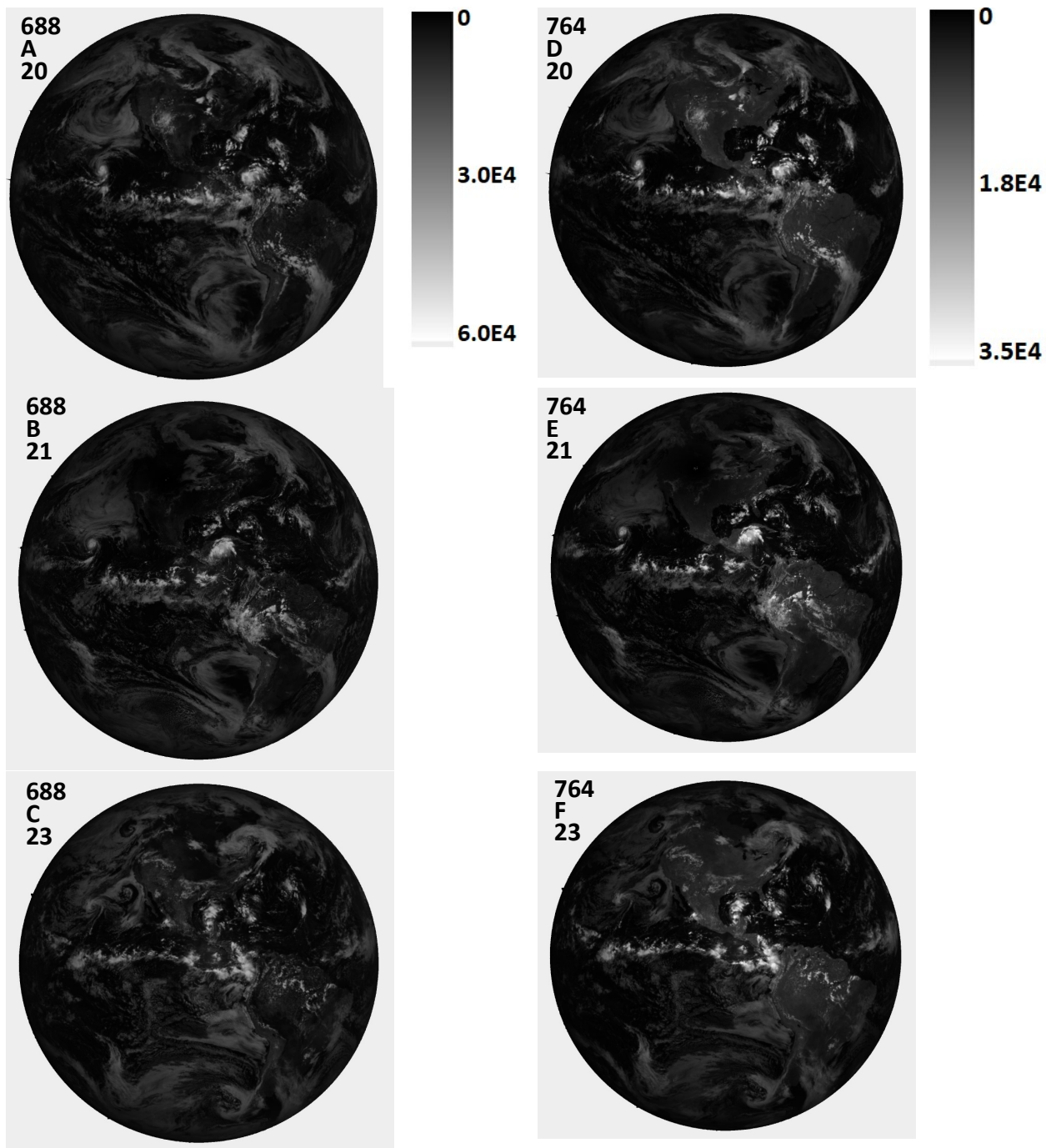
648   **FA2**

Fig. A2b Image in C/s for 688 and 764 nm for 20 Aug., 21 Aug. and 23 Aug. The scale applies to the specific wavelength. North is up.
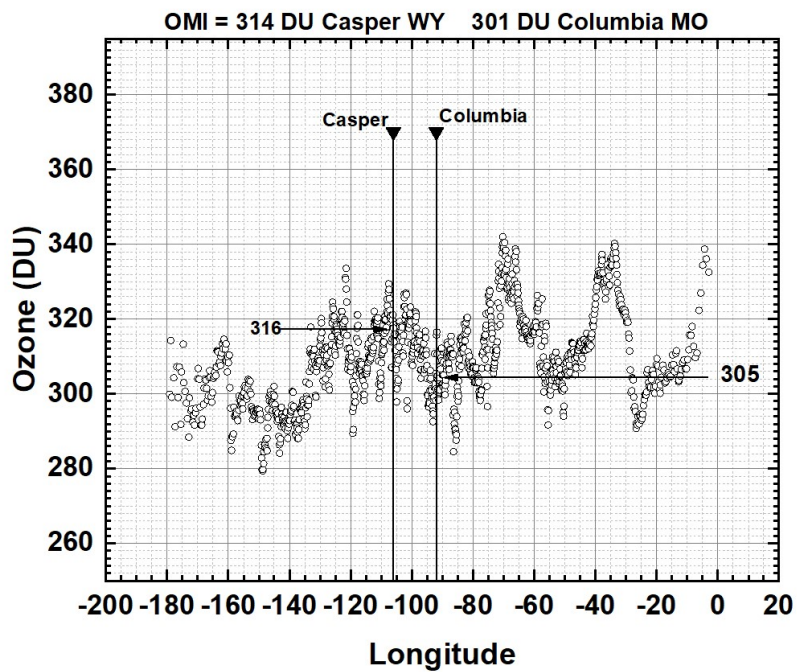
650

651

Fig. A3 EPIC measured ozone amounts from 20 August in the vicinity of Casper, WY and Columbia, MO.

652